

**The Potential for using Geomagnetic Data  
in Ocean and Climate Studies. III:  
Electromagnetic Fields Generated by  
Idealized Ocean Circulation**

**Robert H. Tyler and Lawrence A. Mysak  
C<sup>2</sup>GCR Report No. 94-9  
September 1994**

The Potential for using Geomagnetic Data in  
Ocean and Climate Studies. III:  
Electromagnetic Fields Generated by  
Idealized Ocean Circulation

Robert H. Tyler and Lawrence A. Mysak

September 1994

Department of Atmospheric and Oceanic Sciences  
and  
Centre for Climate and Global Change Research  
McGill University  
805 Sherbrooke St. W.  
Montréal, Québec

## Abstract

Using the induction equation, we investigate the generation of electromagnetic fields by the oceanic advection of ions through the earth's magnetic field. In this report, solutions are presented for a linear induction equation for the magnetic flux density vector which involves prescribed time-independent ocean current and conductivity fields. Once the magnetic flux density is known, the electric field and electric current density are easily obtained by differentiation.

Solutions are given for several examples of idealized flow, including: 1) Vertically and horizontally sheared plane-parallel flow with depth-dependent conductivity; 2) A simple Stommel circulation gyre; and 3) Symmetric gyres. The results indicate that typical ocean current patterns induce magnetic fields that are of detectable magnitudes even far outside of the water. Thus it is concluded that observations of the earth's main magnetic field could be significantly affected by the ocean circulation. Also, the ocean-induced magnetic fields should be especially important in the earth's observed secular (interdecadal and longer) variation since even small-magnitude fields generated by the ocean currents may vary on time scales much shorter than those of inner-earth processes.

# Contents

<b>1</b>	<b>Introduction</b>	<b>1</b>
<b>2</b>	<b>Induction Equation</b>	<b>2</b>
<b>3</b>	<b>Exact Solutions for Steady Idealized Flow</b>	<b>7</b>
3.1	Ocean Surface-Intensified Currents with Horizontal Shear in an Infinitely-Deep Ocean . . . . .	7
3.2	Baroclinic Ocean Currents over an Insulating Seafloor . . . . .	10
<b>4</b>	<b>Solutions of Approximate Equations obtained by Scaling</b>	<b>13</b>
4.1	Horizontal Components . . . . .	15
4.1.1	Horizontal Magnetic Flux . . . . .	19
4.1.2	Horizontal <b>J</b> and <b>E</b> Fields . . . . .	20
4.2	Vertical Component . . . . .	20
4.2.1	Horizontally-Uniform Conductivity . . . . .	21
4.2.2	Horizontally Non-Uniform Conductivity . . . . .	23
4.2.3	Decay Time Scales . . . . .	24
4.2.4	When Vertical Motion is Important . . . . .	26
<b>5</b>	<b>Summary and Discussion</b>	<b>28</b>
<b>A</b>	<b>Appendix: List of Symbols</b>	<b>33</b>
<b>B</b>	<b>Appendix: <i>Matlab</i> Solution</b>	<b>36</b>

# 1 Introduction

In a series of earlier reports (Tyler and Mysak, 1993, 1994a, 1994b) we examined the potential for using geomagnetic data in ocean and climate studies. It is well known that the ocean currents induce electromagnetic fields (*e.g.*, Longuet-Higgins *et al.*, 1954; Sanford, 1971). If the magnetic fields induced by the moving ocean reach geomagnetic observation sites with detectable magnitudes, then the geomagnetic record may contain important information about past and present ocean circulation.

A review of earlier research on and a description of the basics behind electromagnetic induction in the ocean is given, for example, in Filloux (1987), Tyler and Mysak (1993) and the references therein. In brief, seawater contains ions which, as they are advected by the ocean currents through the earth's background magnetic field, are subject to a Lorentz force which tends to induce electrical currents perpendicular to the ocean flow. In the case of a finite-width ocean surface current, electrical currents driven by the Lorentz force in the surface layer short-circuit through the deeper water, creating a closed loop of electrical currents and a consequent magnetic flux through this loop. The question that naturally arises is whether this magnetic field is detectable at geomagnetic observation sites.

Although the basic physics behind electromagnetic induction in the ocean is well established (in fact, most modern ocean current meters operating in a variety of ways rely on these principles), there has been little attempt to describe the electromagnetic fields due to realistic three-dimensional ocean current and conductivity fields. Particularly lacking is a description of ocean-induced electromagnetic fields observed at points outside of the ocean. Such a description, however, is of primary interest to us since most of the geomagnetic record has been taken at land observatories or by satellites outside of the ocean.

The main purpose of this paper is to present a number of analytical solutions for the magnetic field due to idealized ocean current and conductivity fields which

retain detectable magnitudes far away from the ocean. In so doing, we can then argue, as hypothesized above, that the geomagnetic record is likely to contain information about the past and present ocean circulation and climate (since the transport of heat by the ocean currents strongly affects climate, *e.g.*, see Weaver and Hughes, 1992).

The motivation for trying to connect the ocean circulation to geomagnetic records is that the geomagnetic record is in many ways superior to traditional oceanographic data sources. Compared to most forms of oceanographic data, the coverage of magnetic data in time and space is relatively good. In particular, the magnetic coverage is quite good in areas like the Arctic where historically there has been poor oceanographic data coverage. Also, since the low-frequency magnetic fields will reach through sea ice essentially unchanged, satellite coverage of the magnetic field over polar regions (such as taken by MAGSAT) may offer a synoptic view of the ocean dynamics that would be prohibitively expensive to duplicate using traditional *in situ* measurements in these ice-covered regions. (For more on the potential advantages of using geomagnetic data for ocean circulation studies, see Tyler and Mysak (?).)

An outline of this paper is given in the preceding table of contents. Throughout this paper we rely heavily on concepts established in magnetofluidynamics. Since we expect many readers from oceanographic backgrounds will be unfamiliar with these concepts, we have elaborated on the latter where possible. Conversely, readers entirely unfamiliar with rudimentary ocean dynamics may wish to preview the discussion section.

## 2 Induction Equation

In Tyler and Mysak (1994a, 1994b) we derived the set of equations that apply for observers in a rotating (accelerating) reference frame studying electrodynamics of a material medium moving with a velocity relative to the rotating reference

frame. It was assumed that the rotation velocities and velocity of the material medium were much smaller than the speed of light. Considering, in particular, the material medium to be the ocean moving with relative velocity  $\mathbf{u}_c$  in the rotating frame of the solid earth, the constitutive relationships were written as

$$\mathbf{D} = \epsilon(\mathbf{E} - \frac{1}{N^2}\tilde{\mathbf{u}} \times \mathbf{B}), \quad (1)$$

$$\mathbf{H} = \frac{1}{\mu_e}\mathbf{B} - \frac{\epsilon}{N^2}\tilde{\mathbf{u}} \times \mathbf{E}, \quad (2)$$

$$\mathbf{J} = \rho_e\mathbf{u}_c + \sigma(\mathbf{E} + \mathbf{u}_c \times \mathbf{B}) \quad (3)$$

where

$$\tilde{\mathbf{u}} = \mathbf{u}_s + \mathbf{u}_c(1 - N^2), \quad (4)$$

$N = (\mu_r\epsilon_r)^{1/2}$  is the index of refraction, and the solid-body rotation velocity of the earth is

$$\mathbf{u}_s = \Omega r \cos \phi \hat{\lambda} = \Omega r \sin \theta \hat{\lambda}, \quad (5)$$

with  $\Omega$  the rotation rate of the earth,  $r$  the radial coordinate,  $\hat{\lambda}$  the unit vector in the eastward direction,  $\phi$  the latitude and  $\theta$  the colatitude. (See Appendix A for definitions of other symbols.) In the equations above, which are taken from Tyler and Mysak (1994b), lower-case letters were originally used for the electromagnetic vectors measured in the rotating frame to distinguish them from vector measurements made in an inertial frame which were denoted with capital letters. Since it is not necessary in this paper to make this distinction, we have used capital letters in the above equations with the understanding that all measurements are made with respect to the rotating frame of the earth.

Maxwell's equations in the rotating frame were given in Tyler and Mysak (1994a, 1994b) as

$$\nabla \times \mathbf{E} = -\partial_t \mathbf{B}, \quad (6)$$

$$\nabla \cdot \mathbf{B} = 0, \quad (7)$$

$$\nabla \cdot (\epsilon \mathbf{E} - \frac{\epsilon}{N^2} \tilde{\mathbf{u}} \times \mathbf{B}) = \rho_e, \quad (8)$$

$$\nabla \times (\frac{1}{\mu_e} \mathbf{B} - \frac{\epsilon}{N^2} \tilde{\mathbf{u}} \times \mathbf{E}) = \partial_t (\epsilon \mathbf{E} - \frac{\epsilon}{N^2} \tilde{\mathbf{u}} \times \mathbf{B}) + \mathbf{J}. \quad (9)$$

In deriving equations (1)–(9), we neglected  $\frac{(|\mathbf{u}_s|+|\mathbf{u}_c|)^2}{c^2}$ ,  $\frac{|\mathbf{u}_s||\mathbf{u}_c|}{c^2}$ ,  $\frac{|\mathbf{u}_c|^2}{c^2}$  and  $N^{-2} \frac{(|\mathbf{u}_s|+|\mathbf{u}_c|)^2}{c^2}$  relative to 1.

When we consider typical parameter values describing the electric and magnetic properties of the ocean and we avoid very high frequency phenomena (with periods much less than a minute), equation (9) can be approximated by (Tyler and Mysak, 1994a, 1994b)

$$\nabla \times \mathbf{B} = \mu_o \mathbf{J}. \quad (10)$$

Also, it can be easily shown (*e.g.* Tyler and Mysak (1994b)) that for the ocean conditions considered here, the first term on the right-hand side of (3) representing charge advection can be neglected.

Upon combining (6), (10) and the simplified equation (3), we obtain the induction equation

$$\partial_t \mathbf{B} = \nabla \times [\mathbf{u} \times \mathbf{B} - K \nabla \times \mathbf{B}] \quad (11)$$

where  $K = (\sigma \mu_o)^{-1}$  and  $\mathbf{u}$  is the relative velocity of the ocean water ( $= \mathbf{u}_c$  in equations (3) and (4)). Using the vector identities

$$\nabla \times \nabla \times \mathbf{B} = \nabla(\nabla \cdot \mathbf{B}) - \nabla^2 \mathbf{B}, \quad (12)$$

$$\nabla \times (\mathbf{u} \times \mathbf{B}) = (\nabla \cdot \mathbf{B})\mathbf{u} - (\nabla \cdot \mathbf{u})\mathbf{B} + (\mathbf{B} \cdot \nabla)\mathbf{u} - (\mathbf{u} \cdot \nabla)\mathbf{B}, \quad (13)$$

and equation (7), equation (11) can be written (assuming the ocean is also incompressible) as

$$D_t \mathbf{B} = \partial_t \mathbf{B} + \mathbf{u} \cdot \nabla \mathbf{B} = (\mathbf{B} \cdot \nabla)\mathbf{u} + K \nabla^2 \mathbf{B} + K \nabla \ln \sigma \times (\nabla \times \mathbf{B}). \quad (14)$$

Writing (14) out for the three components, we have

$$\begin{aligned} \partial_t B_x + u \partial_x B_x + v \partial_y B_x + w \partial_z B_x &= B_x \partial_x u + B_y \partial_y u + B_z \partial_z u \\ &+ K \partial_x \partial_x B_x + K \partial_y \partial_y B_x + K \partial_z \partial_z B_x \\ &+ K \partial_y \ln \sigma (\partial_x B_y - \partial_y B_x) - K \partial_z \ln \sigma (\partial_z B_x - \partial_x B_z) \end{aligned}$$

(15)

$$\begin{aligned}
\partial_t B_y + u\partial_x B_y + v\partial_y B_y + w\partial_z B_y &= B_x\partial_x v + B_y\partial_y v + B_z\partial_z v \\
&+ K\partial_x\partial_x B_y + K\partial_y\partial_y B_y + K\partial_z\partial_z B_y \\
&+ K\partial_x \ln \sigma(\partial_y B_x - \partial_x B_y) - K\partial_z \ln \sigma(\partial_z B_y - \partial_y B_z)
\end{aligned}$$

(16)

$$\begin{aligned}
\partial_t B_z + u\partial_x B_z + v\partial_y B_z + w\partial_z B_z &= B_x\partial_x w + B_y\partial_y w + B_z\partial_z w \\
&+ K\partial_x\partial_x B_z + K\partial_y\partial_y B_z + K\partial_z\partial_z B_z \\
&+ K\partial_x \ln \sigma(\partial_z B_x - \partial_x B_z) - K\partial_y \ln \sigma(\partial_y B_z - \partial_z B_y)
\end{aligned}$$

(17)

A further discussion of the induction equation, including its representation in other coordinate systems can be found in Tyler and Mysak (1994b). In the general problem of magnetofluidynamics (MFD) (also called magnetohydrodynamics (MHD)), the induction equation (11) is coupled with other equations describing the fields for the conductivity  $\sigma$  and fluid flow  $\mathbf{u}$ . In particular, an electrical force  $\mathbf{J} \times \mathbf{B}$  on the flow will require that the electrodynamics and fluid dynamics be solved for simultaneously. In the case here of ocean induction, however, the electrical forces on the fluid are negligible and the flow field is taken as prescribed. In fact, for typical values of  $\mathbf{B}$  and  $\mathbf{J}$  (that are justified later in the text), we can show that the electrical force on the fluid will typically have a magnitude of about  $|\mathbf{J} \times \mathbf{B}| \approx 4.5 \times 10^{-10} \text{ N/m}^3$ . This would be roughly equivalent in magnitude to the pressure gradient force due to a  $0.5 \mu\text{m}$  sea surface displacement difference between two ends of a large ocean basin such as the Pacific! More typically, such displacements approach a meter. When also considering other dominant forcing mechanisms in the ocean, the electromagnetic forces are clearly negligible and the induction equation can be taken as a differential equation for one vector unknown ( $\mathbf{B}$ ), with prescribed  $K$ ,  $\sigma$  and  $\mathbf{u}$ .

Many useful analogies can be drawn between the terms in this equation and similar terms observed in the vorticity equation of fluid dynamics. The analogies are important since they can suggest useful analytical and numerical techniques that have been developed in fluid dynamics. It should be kept in mind, though, that the physical processes of electromagnetic induction and fluid dynamics are quite different and too strict of an adherence to these analogies can be misleading.

The term on the left-hand side of (14) is the familiar total rate of change of the magnetic field  $\mathbf{B}$ . The first term on the right-hand side is analogous to the stretching/tilting term of fluid dynamics. When the conductivity is uniform, the last term vanishes and the second term can be thought of as a diffusive term.

When  $\sigma$  is not uniform, the Laplacian term describes only part of the magnetic diffusion, the rest being contained in part of the last term. A closer analogy with fluid dynamics arises if we write (14) in the following flux form (in Cartesian coordinates) which can be derived directly from (14) upon using the non-divergence of both  $\mathbf{u}$  and  $\mathbf{B}$ :

$$\begin{aligned}
\partial_t \mathbf{B} &= \nabla \cdot \{u\mathbf{B} - B_x \mathbf{u} + K \nabla B_x - K \partial_x \mathbf{B}\} \hat{x} \\
&+ \nabla \cdot \{v\mathbf{B} - B_y \mathbf{u} + K \nabla B_y - K \partial_y \mathbf{B}\} \hat{y} \\
&+ \nabla \cdot \{w\mathbf{B} - B_z \mathbf{u} + K \nabla B_z - K \partial_z \mathbf{B}\} \hat{z}.
\end{aligned} \tag{18}$$

Equation (18) gives three scalar equations—one for each of the components of  $\mathbf{B}$ . Using the equation for  $B_z$  as an example, we see that the time rate of change of  $B_z$  is described by the divergence of the vector quantity in brackets. Also note that a diffusion term  $\nabla \cdot (K \nabla B_z)$  can now be clearly identified. Still, while we have isolated a ‘diffusion-like’ term, it is somewhat unsatisfactory that the last term  $K \partial_z \mathbf{B}$  in the bracketed expression contains both  $K$  and  $B_z$ . If an analogy with diffusion is desired it might be more meaningful to resort to an anisotropic description of diffusion. The  $B_z$  equation, for example, can be rewritten as

$$\partial_t B_z = \nabla \cdot \{w\mathbf{B} - B_z \mathbf{u} + K \nabla_H B_z - K \partial_z \mathbf{B}_H\} \hat{z}. \tag{19}$$

To interpret the terms in (19) consider a closed volume. We see that the time rate of change of  $B_z$  in the volume depends on the following (taking the terms on the right-hand side of (19) in order):

- 1) Stretching/tilting due to gradients in the vertical velocity  $w$ . This will involve a coupling with the other magnetic components. For example, magnetic fields in the horizontal plane can be tilted by  $w$  to give  $B_z$ ;
- 2) The net advection or flux of  $B_z$  into the volume due to  $\mathbf{u}$ ;
- 3) The *horizontal* diffusive flux of  $B_z$  into the volume;
- 4) A diffusive coupling with the other magnetic components.

We note that the last term in (19) now does not explicitly contain  $B_z$ . This enables us to find solutions to a simplified equation, as will be shown in §4. First, however, we will obtain in §3 exact solutions to the induction equation.

### 3 Exact Solutions for Steady Idealized Flow

#### 3.1 Ocean Surface-Intensified Currents with Horizontal Shear in an Infinitely-Deep Ocean

Consider an infinitely deep ocean in which the ocean current system depicted in Figure 1 is given by the real part of

$$\mathbf{u} = u_o e^{i\lambda y + \mu z} \hat{x} \quad \text{for } z \leq 0, \quad (20)$$

where  $u_o$  is the maximum velocity at the surface,  $\lambda$  is the wave number of the cross-flow shear, and  $\mu^{-1}$  is the vertical decay scale. We consider also a conductivity that is zero outside of the water and decays exponentially with depth from the surface. We thus have

$$\sigma = \begin{cases} \sigma_o e^{\gamma z} & \text{for } z \leq 0 \\ 0 & \text{for } z > 0 \end{cases} \quad (21)$$

where  $\gamma^{-1}$  is the conductivity vertical decay scale.

The reason for including the depth decay in  $\sigma$  is two-fold. First, since for most oceans the temperature decreases with depth, the conductivity also decreases with depth, with a magnitude about twice as great at the surface as compared to that at the bottom (*e.g.* Filloux, 1987). Second, the charge recirculation may be constrained at depth as it would be in the realistic case of a finite-depth ocean (the conductivity of the ocean bottom will be much less than that of sea water).

For simplicity, we first consider a uniform background magnetic field with the northward and vertical components  $F_y, F_z$  respectively. Since there are also no variations assumed in  $\mathbf{u}$  or  $\sigma$  along  $x$ , from (15)-(17) we see that the ocean-induction occurs only along  $x$  and we have  $B_y = F_y, B_z = F_z$ . Then, equation (15) with no time dependence becomes

$$\partial_z \partial_z B_x + \partial_y \partial_y B_x - \partial_z \ln \sigma \partial_z B_x = -\frac{u_o}{K}(i\lambda F_y + \mu F_z)e^{i\lambda y + \mu z}. \quad (22)$$

We will seek solutions for (22) with a  $y$ -dependence of the form  $e^{i\lambda y}$  similar to the forcing on the right-hand side of (22). Hence, if we let  $B_x = Z(z)e^{i\lambda y}$  in (22) and divide through by  $e^{i\lambda y}$  we obtain

$$Z'' - \gamma Z' - \lambda^2 Z = -\frac{u_o}{K}(i\lambda F_y + \mu F_z)e^{\mu z}. \quad (23)$$

We can use the appropriate Green's function to solve (23) in the domain  $-\infty < z \leq 0$ . We first put (23) in a self-adjoint form by multiplying through by  $e^{-\gamma z}$  and combining derivatives. This gives

$$\frac{d}{dz}(e^{-\gamma z} \frac{d}{dz} Z) - \lambda^2 e^{-\gamma z} Z = -(i\lambda F_y + \mu F_z) \frac{u_o}{K_o} e^{\mu z} \quad (24)$$

where  $K_o^{-1} = \mu_o \sigma(z=0) = \mu_o \sigma_o$ .

We must solve (24) subject to two boundary conditions. First, we require

$$Z(z \rightarrow -\infty) = 0 \quad (25)$$

(the ocean can induce no magnetic monopoles). Secondly, in order to have no charge flow across the ocean/air interface we require

$$\mu_o \mathbf{J} \cdot \hat{\mathbf{z}} = (\nabla \times \mathbf{B}) \cdot \hat{\mathbf{z}} = 0 \quad (26)$$

which, since  $\partial_x = 0$  for the geometry of this problem, requires

$$\partial_y B_x(z=0) = i\lambda B_x(z=0) = 0. \quad (27)$$

For non-vanishing  $\lambda$  this can only be satisfied if

$$Z(z=0) = 0. \quad (28)$$

To solve (24) subject to (25) and (28) we construct the following Green's function (see appendix of Tyler and Mysak (1993)):

$$G(z | \xi) = \frac{1}{\beta} \begin{cases} e^{\frac{\gamma+\beta}{2}z} e^{\frac{\gamma}{2}\xi} \sinh\left(\frac{\beta}{2}\xi\right) & -\infty < z \leq \xi \\ e^{\frac{\gamma}{2}z} \sinh\left(\frac{\beta}{2}z\right) e^{\frac{\gamma+\beta}{2}\xi} & \xi \leq z \leq 0 \end{cases} \quad (29)$$

where  $\beta = (\gamma^2 + 4\lambda^2)^{1/2}$ .

Then, the solution of (24) is given by the integral

$$Z = \int_{-\infty}^0 G(z | \xi) (-i\lambda F_o - \mu F_z) \frac{u_o}{K_o} e^{\mu\xi} d\xi, \quad (30)$$

which upon integration gives

$$\begin{aligned} Z(z) = & -(i\lambda F_y + \mu F_z) \frac{u_o}{K_o} \frac{2e^{\frac{\gamma+\beta}{2}z}}{\beta} \left( \frac{1 - e^{(\frac{\gamma+\beta}{2}+\mu)z}}{\gamma + \beta + 2\mu} - \frac{1 - e^{(\frac{\gamma-\beta}{2}+\mu)z}}{\gamma - \beta + 2\mu} \right) \\ & -(i\lambda F_y + \mu F_z) \frac{u_o}{K_o} \frac{2}{\beta} \sinh\left(\frac{\beta}{2}z\right) \left( \frac{1}{\gamma + \beta + 2\mu} e^{(\frac{\gamma+\beta}{2}+\mu)z} \right). \end{aligned} \quad (31)$$

The solution for the induced magnetic field  $B_x$  is then given by the real part of the following expression:

$$B_x \hat{x} = Z e^{i\lambda y} \hat{x}. \quad (32)$$

The contribution from the first term on the right-hand side of (31) can be thought of as due to electrical sources above the observation point while the second is due to sources below. The solution (31) is shown plotted in Figure 2 for parameters typical of the northern mid-latitudes. As will be made clearer in the

next example, the magnetic induction is due to electric currents that move to the left of the current velocity near the surface where the velocity is strong, and recirculate through the deeper water. The maximum vertical electric currents occur where the surface velocities are minimal. While the induction is predominantly due to forcing by the vertical component  $F_z$ , the horizontal component  $F_y$  induces a field that is much weaker (by two orders of magnitude) and out of phase with the  $F_z$  induction, as can be seen in Figure 3. The  $\mathbf{J}$  and  $\mathbf{E}$  fields will be discussed more fully in the next example.

We note that this calculation produces a magnetic field that vanishes outside of the water. This is due to the fact that we have assumed that the ocean currents extend to infinity in the  $x$ -direction with no along-flow variations. In reality, the special geometry producing this cancellation of the magnetic field outside of the water does not occur and we should expect that there will be substantial leakage of the magnetic field into the air, with the returning flux showing a new decay scale that is dependent on the finite length (as well as the width) of the ocean current pattern.

### 3.2 Baroclinic Ocean Currents over an Insulating Seafloor

In contrast to the previous section, we now consider a slightly more realistic example in which the conductivity and velocity can still be written as in (20) and (21) but now it is assumed that below  $z = -H$  we have a motionless and insulating sediment layer (where  $\mathbf{u} = 0, \sigma = 0$ ). The ocean domain therefore is  $-H \leq z \leq 0$ . In this model we can consider pure baroclinic modes if in  $\mathbf{u}$ ,  $\mu$  is allowed to be complex, *i.e.*  $\mu = in\pi/H$  where  $n$  is an integer, and we take a linear combination of  $e^{+\mu z}$  and  $e^{-\mu z}$ .

For some special applications such as the case of a fresh layer over a cooler saline layer, we could consider a conductivity profile that does not decrease monotonically with depth, which can be realized by taking  $\gamma$  to be complex in (21). This could occur since conductivity increases with temperature and salinity, while

the water density decreases with temperature but increases with salinity. Hence, although most of the ocean is stably stratified, this does not imply that conductivity always decreases with depth. However, below we only consider  $\gamma$  to be real.

Mathematically, the difference between this and the last problem is that the boundary condition  $B_x(z \rightarrow -\infty) = 0$  is replaced by  $B_x(z = -H) = 0$ .

The solution is again obtained by the use of Green's functions. Here, though, the integral over the appropriate Green's function has been solved for plotting purposes using the *Symbolic Math* toolbox of *Matlab*. The solutions obtained, while still analytical, are quite long and we have left them in the programming format that was used to produce the plots to be discussed. Thus, the expressions for  $Z$  and  $Z'$  are given in Appendix B.

The solution for the magnetic field is given by

$$B_x = Ze^{i\lambda y}, \quad (33)$$

and using (10) and (3) (with the charge advection term neglected, as discussed in §2) we then obtain the following solutions for the electric current and electric field:

$$J_y = \frac{1}{\mu_o} Z' e^{i\lambda y}, \quad (34)$$

$$J_z = \frac{-i\lambda}{\mu_o} Z e^{i\lambda y}, \quad (35)$$

$$E_y = J_y/\sigma + u_o e^{\mu z} F_z e^{i\lambda y}, \quad (36)$$

$$E_z = J_z/\sigma - u_o e^{\mu z} F_y e^{i\lambda y}. \quad (37)$$

In Figures 4 through 9, we plot the solutions (33)–(37) for various values of the flow and conductivity parameters. In each of the cases we have used the following parameter values typical of mid-latitude background magnetic field and ocean conditions:  $F_y = 3 \times 10^{-5}$  T;  $F_z = -3 \times 10^{-5}$  T;  $u_o = 1$  m/s;  $H = 5 \times 10^3$  m;  $\lambda = 1/(500)$  km<sup>-1</sup>;  $\sigma_o = 5$  S/m. Note we have taken the velocity amplitudes to be of unit value (1 m/s) for convenience, as in §3.1. For the more typical velocity

of .1 m/s in the open ocean, the solutions shown in these figures would have their magnitudes divided by 10.

In each of the Figures 4—9 we have plotted the velocity (solid) and conductivity (dashed) profiles in (a), and in (b)—(c) we have plotted various induced fields which are either in phase (solid) and out of phase (dashed) with the velocity variations in the  $y$  direction. Hence, we see that the surface-intensified current of Figure 4a induces a magnetic field (b) similar in form and magnitude to the solution shown in Figure 2. The dashed line indicates the part of the magnetic field out of phase with the velocity and is due in this case to  $F_y$ . We see that the  $F_y$  induction is negligible, as was found in §3.1. In Figure 4c, we note that the horizontal electric current arising from the Lorentz force in the upper layer is completely compensated by a return current at depth, and in Figure 4d, we observe that the vertical component of the electric current is both much smaller and out of phase. It is important to note that the solution for the horizontal electric field in Figure 4e is independent of depth. The implications of this will be discussed later. Finally, in Figure 4f we see that the vertical electric field is larger than the horizontal electric field. This vertical field is due to  $F_y$ . Hence, although the horizontal background field components of  $\mathbf{F}$  are not, in the cases considered here, effective at creating electric currents and magnetic fields, they do create sizable vertical electric fields.

In Figure 5 we observe that when the flow and conductivity is uniform with depth, the horizontal electric currents  $J_y$  and magnetic field  $B_x$  produced are greatly reduced and out of phase with the velocity. In fact, the small  $F_y$  induction becomes dominant. The electric fields, however are increased.

In Figure 6 we show a baroclinic flow with uniform conductivity. The baroclinic mode is seen to be a highly efficient generator of magnetic fields and electric currents. It was previously thought that measurements of  $\mathbf{E}_H$  indicate the depth-averaged velocity (or conductivity-weighted velocity) (*e.g.* Larsen, 1992; Larsen and Sanford, 1985; Chave and Luther, 1990). Our results, shown in Figure 6e,

however, indicate that baroclinic-type currents can produce horizontal electric fields as strong as those produced by the barotropic mode. Certainly the strength of the  $E_y$  in the case we have solved and plotted here depends on our assumptions of the  $e^{i\lambda y + \mu z}$  dependence of the velocity (with  $\mu = in\pi/H$ ). The real part of this expression describes a baroclinic current that is not only horizontally sheared but also has a phase that varies horizontally. That is, it is a horizontally-sheared baroclinic mode that tilts with depth. When we consider a non-tilting baroclinic current (described, for example, by the real part of  $\mathbf{u} = \frac{1}{2}u_0 e^{i\lambda y}(e^{\mu z} + e^{-\mu z})$ ) the large electrical fields are not obtained.

In Figure 7 and 8 we show the effects of a conductivity profile which decays with depth, and in Figure 9 we show induction due to a higher baroclinic mode with depth-decaying conductivity.

## 4 Solutions of Approximate Equations obtained by Scaling

The radius of the earth is over one thousand times greater than the average depth of the ocean. The fact that induction within the ocean takes place essentially within a thin shell allows us to make approximations that greatly simplify the equations. In the next subsection (§4.1), we use such arguments to obtain the solutions of an approximate set of equations for the horizontal magnetic fields. Then in §4.2 we estimate the vertical magnetic component. Before doing this, however, we will make some general comments about the notation and conventions that we use below.

Unless indicated otherwise, we will work with a Cartesian coordinate system with the components  $x$  (eastward) and  $y$  (northward) occurring in the horizontal plane and  $z$  directed vertically upward. This convention (common in oceanography) should be contrasted with the convention often used in geomagnetic studies in which  $z$  is directed downwards,  $x$  is northward and  $y$  is eastward.

In some cases it is convenient to split the observed magnetic field  $\mathbf{B}$  into two parts, namely,

$$\mathbf{B} = \mathbf{F} + \mathbf{b}, \quad (38)$$

where  $\mathbf{b}$  is that part of  $\mathbf{B}$  generated by the ocean currents and  $\mathbf{F}$  is a background field. All the vectors  $\mathbf{B}$ ,  $\mathbf{b}$ ,  $\mathbf{F}$  have zero divergence.

Further, it is assumed that the electrical current sources of  $\mathbf{F}$  are not located in the ocean or ocean sediments and that  $\mathbf{b}$  (due only to sources within the ocean or sediments) is much smaller than  $\mathbf{F}$  ( $|\mathbf{b}|/|\mathbf{F}| \ll 1$ ). In the standard interpretation, the sources of  $\mathbf{F}$  are located in the earth's core. Hence, according to (10), outside of the core  $\mathbf{F}$  is irrotational ( $\nabla \times \mathbf{F} = 0$ ) and hence using (12) and noting the non-divergence of  $\mathbf{F}$ , we have

$$\nabla \times \nabla \times \mathbf{F} = -\nabla^2 \mathbf{F} = 0. \quad (39)$$

The assumption  $|\mathbf{b}|/|\mathbf{F}| \ll 1$  that we have taken as a working hypothesis deserves special mention. This is consistent with the view that the magnetic fields generated by ocean currents are much smaller than the earth's 'main field' (presumably due to sources at the earth's core). This assumption certainly seems reasonable in most cases (the magnetic fields, as we saw in the examples in §3 were typically tens of nanoteslas compared to the earth's main field which is typically three orders of magnitude greater.) There may, however, be some important exceptions to this assumption, as we will see in §4.2.4 when we discuss the effects of changes in bathymetry. Also, non-steady fields may be quite large and perhaps most importantly, self-excitation modes may exist due to the convergence of conductivity transport at the poles, for example. The latter consideration is beyond the scope of this paper.

As noted after (13), we assume the fluid is incompressible; hence

$$\nabla \cdot \mathbf{u} = 0. \quad (40)$$

Also, vectors as well as operators appearing below with an  $H$  as a subscript refer to the horizontal components (for example,  $\mathbf{u}_H = u\hat{x} + v\hat{y}$  and  $\nabla_H(\cdot) =$

$\partial_x(\cdot)\hat{x} + \partial_y(\cdot)\hat{y}$ ). In the cases where we are explicitly setting  $w = 0$  we will often omit the  $H$  subscript on  $\mathbf{u}$ .

## 4.1 Horizontal Components

Because of the aspect ratio of the ocean, vertical derivatives of the conductivity ( $\sigma$ ) and velocity ( $\mathbf{u}$ ) fields will generally be much larger than the corresponding horizontal derivatives. Hence, the dominant stretching/tilting term in (15) is  $B_z\partial_z u$ . This term is much larger than the advection terms (on the left-hand side) provided both  $\mathcal{H}/\mathcal{L}$  and  $\mathcal{W}/\mathcal{U} \ll 1$  where  $\mathcal{H}$ ,  $\mathcal{L}$ ,  $\mathcal{W}$ ,  $\mathcal{U}$ , are the typical scales for the ocean depth, length, vertical and horizontal velocities, respectively. Since these inequalities hold for the large-scale ocean circulation, the advection terms in (15) can be neglected. This is also true in the equation for  $B_y$  but not necessarily so for the equation for  $B_x$  since the stretching/tilting term involves  $w$ . For  $\mathcal{H}/\mathcal{L} \ll 1$  we also note that the dominant diffusion terms in (15), (16) are those with  $z$  derivatives.

The diffusion time for the horizontal magnetic components will be of order  $\mathcal{H}\mathcal{L}/K \approx 10^3$  seconds or less. Since we are interested in low-frequency processes, we consider  $B_x$  and  $B_y$  to be in a quasi-steady balance and we neglect the time-derivative terms. Note, however, that the diffusion time for the vertical component  $B_z$  may be as large as  $\mathcal{L}^2/K$  and there will be cases, as we will discuss below, where  $\partial_t B_z$  is retained.

Under the above assumptions, equation (15) can be approximated by

$$0 = B_z\partial_z u + K\partial_z\partial_z B_x - K\partial_z \ln \sigma \partial_z B_x. \quad (41)$$

Similar arguments can be made to simplify equation (16) and the two approximate equations for  $B_x$  and  $B_y$  can be written together as the following vector equation:

$$\partial_z(K\partial_z \mathbf{B}_H) = -B_z\partial_z \mathbf{u}_H. \quad (42)$$

Below we will integrate (42) to obtain expressions for  $\mathbf{B}_H$  and  $\mathbf{J}_H$ , our first

we introduce some convenient notation. Let

$$\mathbf{t}_\sigma = \mu_o \sigma \mathbf{u}_H = \mathbf{u}_H / K \quad (43)$$

which can be interpreted as a conductivity transport density  $\sigma \mathbf{u}_H$  multiplied by  $\mu_o$ . The total (dimensionless) conductivity transport through the ocean column of depth  $h$  is then

$$\mathbf{T}_\sigma = \int_{-h}^0 \mathbf{t}_\sigma dz. \quad (44)$$

Also, we define the vertical coordinate

$$s = \frac{-\int_z^0 \sigma dz}{\int_{-h}^0 \sigma dz}, \quad (45)$$

which ranges from  $s = -1$  (at  $z = -h$ ) to  $s = 0$  (at  $z = 0$ ).

In Figure 10b we show an example of  $s$  calculated assuming the  $\sigma$  profile shown in Figure 10a. This example depicts a typical case of a warm shallow current of high conductivity. The ocean below is motionless and has a conductivity slightly greater than half its surface value. A low-conductivity sediment layer extends from the seafloor ( $z = -H$ ) down to  $z = -3H$ . For an insulating ocean floor  $h = H$  and when  $\sigma$  in the water is independent of depth,  $s$  is simply  $s = z/H$ .

To make our results comparable with those of others, we also define

$$\hat{\mathbf{t}}_\sigma = \frac{\mathbf{u}_H^*}{K}, \quad (46)$$

where

$$\mathbf{u}_H^* = \frac{\int_{-h}^0 \sigma \mathbf{u}_H dz}{\int_{-h}^0 \sigma dz} \quad (47)$$

is similar to the notation introduced by Sanford (1971).

Equation (42) is integrated with respect to  $z$  to give

$$K \mathbf{u}_H = \int \mathbf{u}_H dz + C(\mathbf{u}_H) \quad (48)$$

where  $\mathbf{C}$  is an arbitrary vector function of  $x$  and  $y$ . We next divide (48) by  $K$  and take the definite integral between  $z$  and zero, which gives, after rearranging,

$$\mathbf{B}_H = \mathbf{B}_H(x, y, z = 0) + \int_z^0 \frac{1}{K} \left[ \int^{z'} B_z \partial_z \mathbf{u}_H dz - \mathbf{C} \right] dz' \quad (49)$$

The vector  $\mathbf{C}$  is difficult to estimate directly and it is preferable to give the solution in terms of a different undetermined constant  $\Delta \mathbf{B}_H = \mathbf{B}_H(z = 0) - \mathbf{B}_H(z = -h)$ . The  $\mathbf{C} = \mathbf{C}(x, y)$  in (49) can be taken out of the integral, and the equation evaluated at  $z = -h$ ; after rearranging, we obtain

$$\mathbf{C} = \frac{\Delta \mathbf{B}_H + \int_{-h}^0 \left( \frac{1}{K} \int^{z'} B_z \partial_z \mathbf{u}_H dz \right) dz'}{\int_{-h}^0 \frac{dz'}{K}}. \quad (50)$$

The vector  $\mathbf{C}$  describes short-circuiting paths and in fact,  $\mathbf{C}$  is essentially  $\mathbf{J}_{short}/\sigma$  where  $\mathbf{J}_{short}$  is the shorting return electrical current density.

Suppose that electrical currents forced by the Lorentz force in areas of fluid motion are completely compensated by return electrical flow elsewhere in the water column or sediment layer such that the horizontal electrical current density  $\mathbf{J}_H$  integrated over depth  $h$  is zero. In this case,  $\Delta \mathbf{B}_H = 0$ . This is probably a reasonable assumption throughout most of the ocean. However, while realistic solutions for  $\mathbf{B}_H$  may be obtained assuming  $\Delta \mathbf{B}_H = 0$ , calculation of  $B_z$  does not always allow this assumption (see §4.2).

In contrast to the last assumption, we could assume that no short-circuiting occurs (at least through the region considered). This assumption is realized by setting  $\mathbf{C} = 0$ . Two examples where this might be a good assumption are: first, if the flow is barotropic and the conductivity is constant with depth (probably only applicable to shallow well-mixed flow over a flat bottom—a very small percentage of the ocean circulation); second, where there is a horizontal convergence (or divergence) in  $\mathbf{u}$  (or perhaps  $\sigma \mathbf{u}$ ), Lorentz forces may force appreciable electric currents along paths in the horizontal plane with little short-circuiting occurring.

We can simplify (48), (49) and (50) by noting that for realistic ocean currents, we can expect that the variations of  $\partial_z \mathbf{u}_H$  with depth are much greater than the

depth variations of  $B_z$ . This is because  $B_z$  is dominated by the background  $F_z$  which varies only slightly over the thin ocean depth. With this assumption,  $B_z$  can be taken out of the integrals in (48), (49), and (50). Equation (48) (in terms of variables defined above) becomes

$$K \partial_z \mathbf{B}_H = -B_z(\mathbf{u}_H - \mathbf{u}_H^*) + \frac{\Delta \mathbf{B}_H}{\int_{-h}^0 \frac{dz}{K}}, \quad (51)$$

and  $\partial_z \mathbf{B}_H$  (approximately proportional but perpendicular to the horizontal electric current density  $\mathbf{J}_H$ ) can be written as

$$\partial_z \mathbf{B}_H = B_z \left( \frac{\sigma}{\int_{-h}^0 \sigma dz} \mathbf{T}_\sigma - \mathbf{t}_\sigma \right) + \frac{\sigma}{\int_{-h}^0 \sigma dz} \Delta \mathbf{B}_H = -B_z(\mathbf{t}_\sigma - \hat{\mathbf{t}}_\sigma) + \frac{\sigma}{\int_{-h}^0 \sigma dz} \Delta \mathbf{B}_H. \quad (52)$$

Similarly, Equation (49) becomes

$$\begin{aligned} \mathbf{B}_H &= \mathbf{B}_H(z=0) + \int_z^0 \left[ B_z(\mathbf{t}_\sigma - \hat{\mathbf{t}}_\sigma) - (K \int_{-h}^0 K^{-1} dz)^{-1} \Delta \mathbf{B}_H \right] dz' \\ &= \mathbf{B}_H(z=0) + B_z \left( s \mathbf{T}_\sigma + \int_z^0 \mathbf{t}_\sigma dz' \right) + s \Delta \mathbf{B}_H. \end{aligned} \quad (53)$$

We have written equations (52) and (53) in this form since the  $\Delta \mathbf{B}_H$  term will often be assumed to be small enough to neglect. This is because  $\Delta \mathbf{B}_H$  is, to a good approximation, proportional to the average horizontal electric currents in the depth  $h$ . Typically, electric currents induced by the Lorentz force in the regions of  $\mathbf{u}_H$  will short-circuit through deeper water or through the sediment layer rather than through paths in the horizontal plane (*e.g.* Sanford, 1971; Lilley, 1993). Then, the vertically-averaged horizontal electric current is zero and we will generally neglect the  $\Delta \mathbf{B}_H$  term. This assumption seems reasonable except when both the flow is barotropic and  $\sigma$  is independent of depth, which is hardly the case for deep ocean circulation at least. (Also note that all the exact solutions to the idealized models presented in earlier sections, gave  $\Delta \mathbf{B}_H$  exactly zero.)

Under this assumption, and considering  $\mathbf{B}_H(z=0)$  to be known from observation, we see from (53) that for a given  $\mathbf{T}_\sigma$ , the shape and magnitude of  $\mathbf{B}_H$

depend on  $(s + \frac{1}{|\mathbf{T}_\sigma|} \int_{-h}^0 |\mathbf{t}_\sigma| dz)$  which is a function of the baroclinicity of the flow and conductivity structure. An example of this is plotted in Figure 10c.

Also, considering a typical case of deep-water surface-intensified ocean currents, in which case  $\Delta \mathbf{B}_H \approx 0$  and (near the surface)  $|\mathbf{t}_\sigma| \gg |\hat{\mathbf{t}}_\sigma|$ , (52) reduces to

$$\partial_z \mathbf{B}_H \approx -B_z \mathbf{t}_\sigma = -B_z \mathbf{u}_H / K. \quad (54)$$

Equation (54) indicates that measurements of  $\partial_z \mathbf{B}_H$ ,  $B_z$ , and  $\sigma$  within the water would yield an estimate of the absolute velocity of the ocean current.

#### 4.1.1 Horizontal Magnetic Flux

Before proceeding to direct calculations of the vertical magnetic component  $B_z$  in §4.2, we note that the non-divergence of  $\mathbf{B}$  allows us to obtain information about  $B_z$  using the divergence of the horizontal components.

In a similar manner to that given in Tyler and Mysak (1993) we can integrate (53) (assuming, for simplicity,  $\Delta \mathbf{B}_H = 0$  and  $B_z \approx F_z$ ) to obtain the magnetic flux  $\vec{\phi}$  induced between the sea surface and depth  $h$ :

$$\vec{\phi} = \int_{-h}^0 \mathbf{B}_H dz = h \mathbf{B}_H(z=0) + \frac{1}{2} F_z \mathbf{T}_\sigma \tilde{H} \quad (55)$$

where

$$\tilde{H} = 2 \int_{-h}^0 s dz + 2 \frac{1}{|\mathbf{T}_\sigma|} \int_{-h}^0 \int_z^0 |\mathbf{t}_\sigma(z')| dz' dz. \quad (56)$$

The quantity  $\tilde{H}$ , assuming an insulating sediment layer, is  $\tilde{H} \approx H - D$  for a shallow ocean current (of thickness  $D$ ) over deep water, and  $\tilde{H} \rightarrow 0$  as  $\mathbf{u}$  and  $\sigma$  becomes uniform with depth.

From the non-divergence of  $\mathbf{B}$ ,

$$\int_{-h}^0 \nabla_H \cdot \mathbf{B}_H dz = \nabla_H \cdot \vec{\phi} = -B_z(z=0) + B_z(z=-h) = -\Delta B_z. \quad (57)$$

Equation (57) gives an expression for the difference in  $B_z$  across the depth  $h$  due to leakage of the horizontal magnetic components  $B_H$ . Such expressions are

useful when comparing with data (mostly taken outside of the ocean). In the general case where  $\Delta \mathbf{B}_H \neq 0$  simple expressions such as this are not possible.

#### 4.1.2 Horizontal $\mathbf{J}$ and $\mathbf{E}$ Fields

Consider the flow  $\mathbf{u}_H$  to be in the  $x$  direction. The scaling arguments presented at the beginning of this section suggest that an approximate version of (10) for this case is

$$\partial_z B_x = \mu_o J_y. \quad (58)$$

We can use (52) in (58) to solve for the horizontal electric current  $J_y$  where, as discussed earlier, we assume that the depth-averaged  $\mathbf{J}_H$  over  $h$  is zero. Hence,  $\Delta \mathbf{B}_H = 0$ . We then have

$$J_y = -\frac{B_z}{\mu_o}(t_\sigma - \hat{t}_\sigma). \quad (59)$$

Then, using (59) in Ohm's law (equation (3), which, for this case and with the charge advection term neglected, would be  $E_y = J_y/\sigma + uB_z$ ) we have an expression for the horizontal electric current

$$E_y = B_z u^*, \quad (60)$$

which, for  $B_z \approx F_z$  agrees with the results found by Sanford (1971). This interesting result—that the horizontal electric field is independent of depth—also was found in the exact solutions for the problems presented in §3.

## 4.2 Vertical Component

To seek solutions for the vertical component, we start with the simplest case in which the conductivity is horizontally uniform (§4.2.1) and then consider increasingly more complicated (§4.2.2) cases.

### 4.2.1 Horizontally-Uniform Conductivity

Consider  $\sigma$  independent of  $x$  and  $y$ , and  $w = 0$ . Then the  $z$ -component of (18) (or (17)) can be written as

$$D_t B_z = K \nabla^2 B_z. \quad (61)$$

Now further assume  $\partial_t B_z = 0$ . Then, (61) reduces to

$$\mathbf{u}_H \cdot \nabla B_z = K \nabla^2 B_z \quad (62)$$

or,

$$\nabla^2 B_z = \mathbf{t}_\sigma \cdot \nabla B_z. \quad (63)$$

Substituting  $B_z = F_z + b_z$ , using (39) and making the assumption  $|\mathbf{t}_\sigma \cdot \nabla b_z| \ll |\nabla^2 b_z|$ , (63) becomes the 3D Poisson equation

$$\nabla^2 b_z = \mathbf{t}_\sigma \cdot \nabla F_z. \quad (64)$$

The general solution to (64) in closed form is found using the Green's function for this equation (together with the requirement that  $b_z \rightarrow 0$  away from the source areas):

$$G(x, y, z | \xi, \eta, \zeta) = -\frac{1}{4\pi} ((x - \xi)^2 + (y - \eta)^2 + (z - \zeta)^2)^{-1/2}$$

(see (?), page 153). The solution for  $b_z$  is then

$$b_z = -\frac{1}{4\pi} \iiint \frac{\mathbf{u}_H(\xi, \eta, \zeta) \cdot \nabla F_z(\xi, \eta, \zeta) d\xi d\eta d\zeta}{K(\xi)} ((x - \xi)^2 + (y - \eta)^2 + (z - \zeta)^2)^{-1/2}. \quad (65)$$

If the flow is barotropic and the conductivity is also uniform with depth we can replace (65) by an area integral:

$$b_z = -\frac{1}{4\pi} \iint \frac{1}{K} \mathbf{u}_H(\xi, \eta) \cdot \nabla F_z(\xi, \eta) \ln \frac{z + H + ((x - \xi)^2 + (y - \eta)^2 + (z + H)^2)^{1/2}}{z + ((x - \xi)^2 + (y - \eta)^2 + z^2)^{1/2}} d\xi d\eta, \quad (66)$$

where  $H$  is the depth of the ocean. Tyler and Mysak (1993) plotted the solution for induction by a barotropic double gyre. Here, we will further consider two

more cases.

The first case we will consider is that of the familiar wind-driven Stommel gyre (see, for example, Abarbanel and Young (1987)). We choose the stream function for the ocean velocity associated with this gyre to be defined by the approximate boundary layer solution  $\psi = \psi_o \pi (1 - e^{-15x/X} - x/X) \sin(\pi y/Y)$  where the scale length  $X = Y = 10^7$  m and we consider the domain  $0 < x < X, 0 < y < Y$ . The stream function (taking  $\psi_o = X$  m/s =  $10^7$  m<sup>2</sup>/s) as well as a surface plot of the northward velocity is shown in Figure 11.

We assume  $\mathbf{u}_H \cdot \nabla F_z = \beta_m v$  (where  $\beta_m = \partial_y F_z \approx -10^{-12}$  T/m),  $H = 500$  m, and  $\sigma = 6$  (S/m) and solve (66) numerically using a gaussian quadrature program in the numerical integration toolbox written for *Matlab*. Solving the integral for a field of points is rather time-consuming when the points are near the ocean surface since the integrand has a singular behavior and more quadrature coefficients must be used for sufficient accuracy. To show the basic form of the field, we have evaluated the field at an altitude of 10 km. This is shown in Figure 12. We see that the maximum  $b_z$  occurs in the area of strong northward velocities and the magnitude is of order 10 nT (though this is probably an over-estimate since the values for the transport we chose are probably on the high side). Considering the assumptions we made, the only mechanism creating the  $b_z$  observed in Figure 12 is that of advection of the ‘planetary magnetism’  $F_z$  by the northward velocity  $v$ .

Now we will consider a simple case that will allow us to estimate the dependence of the magnitude of  $b_z$  on the depth and length scales of the flow. We consider an ocean velocity that can be described by a sum of modes of the form

$$\mathbf{u} = \mathbf{u}_o e^{i(kx+ly)} \quad (67)$$

where  $\mathbf{u}_o = u_o \hat{x} + v_o \hat{y}$  is a vector in the horizontal plane that is uniform within the layer  $-D \leq z \leq 0$  and zero outside of this layer. For simplicity, we also consider the conductivity  $\sigma$  to be uniform within the layer  $-D \leq z \leq 0$ .

As before, we consider a forcing due solely to the advection of planetary magnetism. Hence, (64) becomes

$$\nabla^2 b_z = \mathbf{t}_\sigma \cdot \nabla F_z = -\frac{v}{K} \beta_m = -\frac{v_o e^{i(kx+ly)}}{K} \beta_m \quad (68)$$

where  $v_o$  is the northward component of  $\mathbf{u}_o$  which is zero for  $z > 0$  and  $z < -D$ .

Equation (68) is easily solved by first using the separation of variables technique (i.e., putting  $b_z \propto e^{i(kx+ly)}$ ) and then using the familiar Green's function techniques to solve the resulting ODE involving  $z$  in the domain  $|z| < \infty$  and imposing the boundary conditions that  $b_z$  remain bounded at  $z = \pm\infty$ . The solution (using  $\kappa = (k^2 + l^2)^{1/2}$ ) is

$$\mathbf{b}_z = -\frac{v_o \beta_m}{2K \kappa^2} e^{i(kx+ly)} \begin{cases} e^{-\kappa z} (1 - e^{-\kappa D}) & \text{for } z \geq 0 \\ 2 - e^{\kappa z} - e^{-(\kappa z + \kappa D)} & \text{for } -D \leq z \leq 0 \\ -e^{\kappa z} (1 - e^{+\kappa D}) & \text{for } z \leq -D \end{cases} \quad (69)$$

To plot some examples, we assume  $D = 5000$  m,  $\sigma = 5$  S/m (within the water)  $l = 0$  and  $k = 2\pi/2000$  1/m. The velocity magnitude  $v_o$  appears as a multiplier (taken to be 1 m/s, for simplicity). The velocity vectors are shown in Figure 13 while  $b_z$  can be seen in 14. In Figure 15 we have created a field of gyres using a linear sum of velocities of the form (67) with  $k = l = \pm 2\pi/2000$  1/m (i.e., the real parts of  $u = \frac{i}{2}(e^{i(kx+ly)} + e^{i(kx-ly)})$ ,  $v = -\frac{i}{2}(e^{i(kx+ly)} - e^{i(kx-ly)})$ ). The induced steady-state field  $b_z$  is seen in Figure 16.

Figure 17, which uses the same values for the parameters as in Figures 13–16, shows the amplitude of  $b_z$  as a function of the current thickness  $D$  and the wavenumber  $\kappa$ .

#### 4.2.2 Horizontally Non-Uniform Conductivity

Equation (19) governing  $B_z$  involves the unknown horizontal components  $\mathbf{B}_H$  in two terms. The first term, involving  $w$ , we at first neglect while considering a flow with  $w = 0$  (a flow where  $w \neq 0$  is considered in §4.2.4). The second term,  $K \partial_z \mathbf{B}_H$ , can be obtained from the equations for the horizontal magnetic

components. We use (51) for  $K\partial_z\mathbf{B}_H$  in (19). This gives

$$\partial_t B_z = \nabla \cdot (K\nabla_H B_z) - \nabla \cdot \left( B_z \mathbf{u}_H^* + \frac{\Delta \mathbf{B}_H}{\int_{-h}^0 dz/K} \right). \quad (70)$$

When  $\Delta \mathbf{B}_H = 0$ , (70) reduces to an advection-diffusion equation for  $B_z$  and may be solved by standard techniques. Often, however, the horizontal diffusion term  $\nabla \cdot (K\nabla_H B_z)$  will be very small (especially for large-scale ocean features away from the coasts) and the dominant steady-state balance is

$$\nabla \cdot \left( B_z \mathbf{u}_H^* + \frac{\Delta \mathbf{B}_H}{\int_{-h}^0 dz/K} \right) = 0. \quad (71)$$

Since  $\Delta \mathbf{B}_H$  is irrotational ( $\Delta \mathbf{B}_H = \mathbf{B}_H(z=0) - \mathbf{B}_H(z=-h)$  involves  $\mathbf{B}_H$  on two surfaces with no normal electrical current, by assumption; hence, by (10)  $\nabla \times \Delta \mathbf{B}_H = 0$ ), it can be written as the gradient of a scalar, say  $\Delta \mathbf{B}_H = \nabla P$ , where  $P = P(x, y)$ . Also, making the approximation  $B_z \approx F_z$  as before, (71) becomes a 2D scalar equation for the one unknown variable  $P$ :

$$\nabla^2 P - \nabla \ln \left( \int_{-h}^0 dz/K \right) \cdot \nabla P = - \int_{-h}^0 dz/K \nabla \cdot (\mathbf{u}_H^* F_z). \quad (72)$$

Given a realistic conductivity field and current data (72) can be easily solved using numerical techniques.

### 4.2.3 Decay Time Scales

In the examples we have presented so far, we have assumed steady-state conditions for  $B_z$ . This assumption is valid when the time scales considered are much longer than the magnetic diffusion time  $\tau_d$ . An estimate of  $\tau_d$  can be obtained by comparing the time rate of change term  $\partial_t B_z$ , to the magnetic diffusion term,  $K\nabla^2 B_z$ , in equation (61). Since  $\nabla^2 B_z = \nabla_H^2 B_z + \partial_z \partial_z B_z = \nabla_H^2 B_z + \partial_z (-\nabla_H \cdot \mathbf{B}_H)$  (using the non-divergence of  $\mathbf{B}$ ), the largest component of  $\nabla^2 B_z$  likely scales as  $|\mathbf{b}|/(\mathcal{L}\mathcal{H})$  (not  $|\mathbf{b}|/\mathcal{H}^2$ ), where  $\mathcal{L}$  is a typical horizontal length scale and  $\mathcal{H}$  is a typical depth scale. Taking  $|\partial_t B_z| \approx |\partial_t \mathbf{b}|$  we find that diffusion will be more

important than the time rate of change for time scales larger than

$$\tau_d \approx (\mathcal{L}\mathcal{H})/K. \quad (73)$$

The magnetic diffusion coefficient is  $K \approx 10^5$  in the ocean. The maximum value for  $\tau_d$  can be estimated using the maximum values for  $\mathcal{L}$  ( $\leq 10^7$  m) and  $\mathcal{H}$  ( $\leq 10^4$  m), giving  $\tau_d \approx 10^6$  s ( $\approx 12$  days). We will now present a calculation that verifies that (73) is a reasonable estimate.

In §4.2.1 we used simplified equations for  $b_z$  assuming a steady-state. Using similar assumptions but leaving in the time-derivative term we obtain

$$\partial_t b_z - K \nabla^2 b_z = -\mathbf{u}_H \cdot \nabla F_z \quad (74)$$

where  $b_z$  and the forcing term (on the right-hand side of (74)) are now functions of  $(x, y, z, t)$ . Assuming  $K$  is uniform in space and constant in time,  $b_z(x, y, z, t = 0) = 0$ , and requiring  $b_z$  to be bounded, (74) has the solution

$$b_z = \int_0^t \int_V \frac{1}{(2\sqrt{K\pi t})^3} e^{-\frac{(x-\xi)^2 + (y-\eta)^2 + (z-\zeta)^2}{4Kt}} f(\xi, \eta, \zeta, t) d\xi d\eta d\zeta dt \quad (75)$$

where  $V$  is all space containing  $f$  and  $f(\xi, \eta, \zeta, t)$  is the forcing function expressed on the right-hand side of (74).

If  $f$  is harmonic in the horizontal plane (i.e.,  $f \propto e^{i(kx+ly)}$  (or can be decomposed into such modes)), the solution to (74) is instead

$$\mathbf{b}_z = e^{i(kx+ly)} \int_0^t \int_{-\infty}^{\infty} \frac{1}{2\sqrt{K\pi t}} e^{-k^2 \kappa t} e^{-\frac{(z-\xi)^2}{4Kt}} f d\xi dt. \quad (76)$$

For  $f = -v_o \beta_m e^{i(kx+ly)}$  for  $t > 0$  and  $-D < z < 0$  and  $f = 0$  otherwise, the integral over  $z$  in (76) can be solved giving

$$\mathbf{b}_z = e^{i(kx+ly)} \int_0^t \frac{v_o \beta_m}{2} \left[ \operatorname{erf} \left( \frac{z}{2\sqrt{Kt}} \right) e^{-k^2 K t} - \operatorname{erf} \left( \frac{D+z}{2\sqrt{Kt}} \right) e^{-k^2 K t} \right] dt. \quad (77)$$

We evaluated (77) numerically for several choices of typical values of the parameter to obtain the magnitude of  $\mathbf{b}_z$  at the surface ( $z = 0$ ) for several values

of  $t$ . The results indicate that the magnetic diffusion time as expressed by (73) is good as a rough indication. For example, using  $z = 0$ ,  $D = 10$  km,  $k = 2\pi/3000$  1/km,  $\sigma = 5$  S/m, and  $v_o = 1$  m/s, the magnitude of  $b_z$  had reached about 10 percent its steady-state magnitude after  $1\tau_d$ , 50 percent after  $5\tau_d$ , and by  $20\tau_d$ ,  $b_z$  had essentially reached steady-state.

Note that the arguments presented in this section apply to the setup/decay time scales for  $B_z$ . We expect that the time-scales associated with  $\mathbf{B}_H$  (within the ocean, at least) will be much shorter because the diffusion term will scale as  $|\mathbf{b}|/\mathcal{H}^2$ .

#### 4.2.4 When Vertical Motion is Important

In some cases, particularly for barotropic flow over realistic bathymetry, the vertical velocity  $w$  cannot be neglected. We will now derive an equation for  $B_z$  which although it does not involve  $w$  directly, it takes the vertical motion into account. The derivation is analogous to that leading to the potential vorticity equation in fluid dynamics.

Consider a scalar fluid property  $\lambda$  which satisfies the equation

$$D_t\lambda = \Psi \quad (78)$$

where  $\Psi$  is a source function for  $\lambda$ . We shall also use the identity

$$\mathbf{B} \cdot D_t\nabla\lambda = (\mathbf{B} \cdot \nabla) D_t\lambda - (\mathbf{B} \cdot \nabla\mathbf{u}) \cdot \nabla\lambda \quad (79)$$

(see Pedlosky, 1979 pp. 38). Taking the dot product of the induction equation (14) with  $\nabla\lambda$ , adding the result to (79), and using (78) we have

$$D_t(\mathbf{B} \cdot \nabla\lambda) = \mathbf{B} \cdot \nabla\Psi + \nabla\lambda \cdot (K\nabla^2\mathbf{B} + K\nabla\ln\sigma \times (\nabla \times \mathbf{B})). \quad (80)$$

For incompressible barotropic flow in a fluid of thickness  $H_l + \eta$ , the status function  $(\frac{z-H_l}{H_l+\eta})$  (see Pedlosky, 1979, pp. 63) is conserved following the fluid, where  $z - H_l$  is the height above the bottom of the layer (located at  $z = -H_l$ ) and  $\eta$

is the displacement from the mean depth of the top surface of the layer. This result applies to a barotropic layer bound by material or fluid surfaces. In many oceanic cases, the bottom surface is the seafloor (hence  $H_l = H$  is the depth of the water), and  $\eta$  is neglected (nondivergent approximation). Alternatively, the bottom of the layer is described by the pycnocline (a material surface separating lighter surface water from denser water below) in which case  $H_l$  could be the thickness of the surface wind-driven mixed layer.

Now consider  $\lambda$  in (80) to be the status function, so that  $\Psi = 0$ . Because of the aspect ratio of the ocean, we expect that to order  $\mathcal{H}/\mathcal{L}$ , the dominant component of  $\nabla(\frac{z-H_l}{H_l+\eta})$  will be the vertical component. Also, within the barotropic layer, provided the  $\sigma$  variations with depth are not extreme, the horizontal components of the ocean-current induced magnetic fields will be weak. Hence, we expect that when these assumptions hold, a good approximation to (80) can be written as

$$D_t(B_z/H_l) = \frac{1}{H_l} (\nabla \cdot \{K \nabla B_z - K \partial_z \mathbf{B}\}) = \frac{1}{H_l} (\nabla \cdot \{K \nabla_H B_z - K \partial_z B_H\}), \quad (81)$$

where we used  $\nabla \lambda = \nabla(\frac{z-H_l}{H_l+\eta}) \approx \frac{1}{H_l} \hat{z}$  and the  $z$ -component of (18).

Equation (81) shows that following the fluid, the changes in  $B_z/H_l$  are due to magnetic diffusion and a diffusive coupling with the horizontal magnetic components when  $\sigma$  is not uniform.

As a specific example, consider a mixed layer where  $\sigma = \sigma(z)$ . Then (81) reduces to

$$D_t(B_z/H_l) = \partial_t(B_z/H_l) + \frac{\mathbf{u}}{H_l} \cdot \nabla B_z - B_z \frac{\mathbf{u}}{H_l} \cdot \nabla \ln H_l = \frac{1}{H_l} (K \nabla^2 B_z). \quad (82)$$

For steady-state we see that after putting  $B_z = F_z + b_z$  and multiplying through by  $H_l/K$ , (82) is similar to equation (64) already studied except for the addition of another forcing term  $-F_z \mathbf{t}_\sigma \cdot \nabla \ln H_l$ . This new forcing term, however, may be greater than the forcing term  $\mathbf{t}_\sigma \cdot \nabla F_z$  by a factor  $R_e \alpha / H_l$  where  $\alpha$  is the slope ( $\alpha = |\nabla H_l|$ ) and  $R_e$  (the radius of the earth) is the scale over which  $F_z$  varies.

In the case that  $H_l$  represents the depth of the ocean, steep bottom slopes have a magnitude of about  $\alpha \approx 10^{-2}$ , the radius of the earth  $R_e$  is 6371 km while

the depth  $H$  is typically 5 km, giving  $R_e\alpha/H_l \approx 10$ . Thus in regions of steep topography, variations in  $H$  could be more important than the advection of  $F_z$  in inducing  $b_z$ . In shallow water topographic forcing may even generate much stronger fields than those generated by the advection of planetary magnetism. Similar conclusions can be reached when  $H_l$  is taken to represent, for example, the depth of the mixed surface layer. We note that for cases where the variations in  $H_l$  are comparable in magnitude to the average  $H_l$ , the simplifying assumptions used above should be reexamined.

Upon comparing (82) (for steady-state) with (64), we see that the  $B_z$  solutions for the familiar wind-driven Stommel gyre could have been similarly induced by a linearly varying  $H_l$  rather than a linear variation in  $F_z$ . This is analogous to the finding in fluid dynamics in which the “ $\beta$ -effect” (due to an assumption of a linear variation in the rotation parameter) is similar to the effect of a sloping  $H_l$ .

## 5 Summary and Discussion

Using a magnetofluiddynamic approach, we have investigated electromagnetic induction in the ocean. Since the electrical forces on the fluid are extremely small for the case of the ocean circulation, the velocity field can be prescribed and the induction equation reduces to a governing equation for one unknown vector variable—the magnetic field.

In section §3, we found exact solutions to the induction equation for some idealized flows. The results gave magnitudes of about 10–100 nT for the magnetic field  $\mathbf{b}_H$ , about  $10^{-5}$  V/m for the electric fields  $\mathbf{E}$ , and about  $10^{-5}$  A/m<sup>2</sup> for the electric current density  $\mathbf{J}$  induced by the ocean currents.

In section §4.2 we solved an approximation equation and obtained motionally-induced vertical magnetic fields usually of order 1 – 10 nT but perhaps reaching 100’s of nT for some cases. The results also indicate that the decays scales for the magnetic field away from the ocean are of the same order as the horizontal scale of the flow, which allows magnetic effects to be observable thousands of

kilometers inland. The magnetic diffusion time in the ocean is found to be less than about 10 days even in the most extreme cases. Hence ocean electrodynamics on much longer time scales is in quasi-static balance with the ocean currents and conductivity field.

It is not possible to give a unified description of electromagnetic induction that will apply to all cases of motional induction in the ocean. It is, however, possible to describe what typically occurs. The electromagnetic induction is generally driven by a combination of three fields (the conductivity  $\sigma$ , the ocean current velocity  $\mathbf{u}$ , and the background vertical component of the earth's magnetic field  $F_z$ ) and their derivatives.

The conductivity of seawater depends on both temperature and salinity. Given the range of temperatures and salinities in the ocean, it can be noted (Filloux, 1987; Tyler, 1992; Tyler and Mysak, 1993) that outside of the polar regions  $\sigma$  varies principally with temperature. Within the polar regions, the situation is often reversed, with the temperature very near to freezing ( $\approx -2^\circ \text{C}$ ) and the salinity having large variations due to brine rejection during ice formation and, in the case of the Arctic, due to large and variable river discharge. Hence, in polar regions  $\sigma$  can be principally dependent on salinity.

Over most of the ocean, warm surface waters have a conductivity roughly twice as great as that at depth. The warm surface layer is also roughly coincident with the strong mid-latitude wind-driven ocean gyres. The average depth of the ocean is about 4 km, while the surface layer thickness is usually less than 500 m and, for the mixed layer, more typically about 100 m. Typical current speeds are 0.1 m/s. There are, however, certainly exceptions. Boundary currents, for example, can have very large velocities (exceeding 1 m/s) near the surface and may extend nearly to the ocean floor.

The conductivity of the wet sediments may reach magnitudes about a tenth that of seawater. Also, the atmosphere (below the ionosphere) can usually be treated as an insulator. Finally the conductivity of sea ice depends highly on the

brine content, but usually it is less than a tenth that of seawater. A map showing  $\sigma$  for the global ocean surface as well as a chart showing the dependence of  $\sigma$  on salinity and temperature can be found in Tyler and Mysak (1993).

The vertical component of the earth's background field  $F_z$  is shown in Figure 18. The magnitude varies from about 60,000 nT ( $= 6 \times 10^{-5}$  T) at the poles to zero at the magnetic equator.

In the northern magnetic hemisphere,  $F_z$  is directed downward. Hence, in a typical case, the Lorentz force  $\mathbf{u} \times \mathbf{F}$  tends to create an electrical current perpendicular and to the left of the ocean current velocity. Short-circuiting occurs through deeper water creating a closed circuit and magnetic flux through this circuit. In this case, the induced horizontal magnetic field  $\mathbf{b}_H$  is strongest at the interface between the surface and deeper layers (where the maximum velocity shear occurs) and is directed in a direction opposite to that of the ocean velocity. (In the southern magnetic hemisphere, the sign of  $F_z$  is reversed and  $\mathbf{b}_H$  would be directed in the same direction as the velocity.)

To have an ocean-induced vertical magnetic component  $b_z$  we require that at least one of  $\sigma$ ,  $F_z$ ,  $\mathbf{u}$  varies horizontally. This is generally the case in practice. The examples of  $b_z$  we have derived in this paper were forced by functions with simple and smooth variations (*e.g.* forcing due to advection of planetary magnetism assumed smooth variations in  $F_z$ ). Sharper variations exist in the ocean and probably generate  $b_z$  fields (perhaps unsteady) much larger than the  $b_z$  fields we have calculated).

There are two ways of thinking of  $b_z$  induction. In the first case,  $b_z$  is generated due to a convergence in the horizontal magnetic flux  $\vec{\phi}$ , as discussed in §4.1.1. Note that in this case, the  $b_z$  at the sea surface and sea floor may be in opposite directions. Also, this type of induction of  $b_z$  does not occur in a barotropic fluid (when  $\sigma$  is also uniform over  $h$ ) since  $\vec{\phi}$  for this case is zero.

In the second type of  $b_z$  induction, electrical currents short-circuit in the horizontal plane rather than in a plane containing the vertical axis. This type of

induction is most efficient when the flow is barotropic (and  $\sigma$  is uniform over  $h$ ). Also, note that  $b_z$  due to this induction must have the same direction at the sea surface and at the seafloor.

We have presented arguments which indicate that for uniform ocean conductivity  $\sigma$ , barotropic currents are efficient generators of electric fields but poor generators of electrical current and magnetic fields, while baroclinic currents are efficient generators of electrical current and magnetic fields, and (in our simple examples) poor generators of electric fields. When, however, we include a consideration of the vertical dependence of  $\sigma$  it appears that virtually all realistic forms of ocean circulation will be reasonably efficient generators of electrical current and magnetic fields. Also, these magnetic fields do not remain confined to the ocean and probably have detectable magnitudes thousands of kilometers away from the ocean. Typical steady ocean circulation features should induce magnetic fields of order 10 nT outside of the ocean, while fields within the ocean may be an order of magnitude greater.

An important point should be made about the underlying assumption  $|\mathbf{b}| \ll |\mathbf{F}|$  which we have made repeatedly in the analyses. From a preliminary inspection of large-scale steady induction problems, this assumption seems valid since the typical magnitudes of the ocean-induced magnetic fields are several orders of magnitude less than that of the earth's background field  $\mathbf{F}$ . In making this assumption, however, we are not allowing for the possibility of a positive feedback of  $\mathbf{b}$  onto  $\mathbf{F}$ . Or, stated another way, we do not allow for 'self-excitation' or dynamo modes. Our current research indicates, however, that there may be cases where feedback is important, particularly in regions where there is a net flux of conductivity. On a global scale, systematic ocean effects such as the poleward transport of conductivity may be extremely important in establishing  $\mathbf{F}$  as well as  $\mathbf{b}$ .

## Acknowledgements

This work was supported by research grants awarded to LAM from NSERC, AES, and Fonds FCAR. Helpful discussions with Dr. P. Lorrain are gratefully acknowledged.

## A Appendix: List of Symbols

**B** magnetic flux density (T)

**H** magnetic field strength (A/m)

**J** electric current density ( $A/m^2$ )

**D** electric flux density ( $C/m^2$ )

$\rho_e$  electric volume charge density ( $C/m^3$ )

**E** electric field strength (V/m)

$\mu_e = \mu_r \mu_o$  magnetic permeability (H/m)

$\mu_o = 4\pi \times 10^{-7}$  magnetic permeability of free space (H/m)

$\mu_r$  relative magnetic permeability (dimensionless, and in this report taken to be = 1 everywhere)

$\epsilon = \epsilon_r \epsilon_o$  electric permittivity (F/m)

$\epsilon_o = 8.854 \times 10^{-12}$  electric permittivity of free space (F/m)

$\epsilon_r$  relative electric permittivity of material (dimensionless), ( $\epsilon_r \approx 80$  for seawater)

$N = (\mu_r \epsilon_r)^{1/2}$  (dimensionless) index of refraction

$\sigma$  electric conductivity (S/m)

$c = (\mu_o \epsilon_o)^{-1/2}$  speed of light  $\approx 3 \times 10^8$  (m/s)

$K = (\sigma \mu_o)^{-1}$  magnetic diffusivity ( $m^2/s$ )

**b** =ocean-induced component of magnetic flux density (T)

**F** =background component of magnetic flux density (T)

$\omega$  = angular velocity of solid-body rotation

$\Omega = 2\pi/day \approx 7.3 \times 10^{-5}$  (radians/s) rotation rate of the earth

$R_E \approx 6370$  km, radius of earth

$D_t$  total derivative the fluid)

$\mathbf{u} = u\hat{x} + v\hat{y} + w\hat{z}$  velocity of ocean currents

$\vec{\phi}$  horizontal magnetic flux (horizontal magnetic field integrated through depth of ocean)

$u_o$  ocean velocity at surface

$\mu$  depth decay factor of flow

$\gamma$  depth decay factor of conductivity

$\lambda$  horizontal wave number of ocean current shear

$$\beta = (\gamma^2 + 4\lambda^2)^{1/2}$$

$H$  depth of ocean

$h$  total depth of ocean and sediment layer

## Units

S = siemens = A/V

Wb = webers = V · s

H = henries = Wb/A

F = farads = C/V

C = coulombs

A = amperes = C/s

T = teslas = Wb/m<sup>2</sup>

V = volts

s = seconds

m = meters

## B Appendix: *Matlab* Solution

Below we give the *Matlab* output for the analytical solutions for  $Z$  ( $Z$ ) and  $Z'$  ( $Z_p$ ) as discussed in §3.2. (To convert to the notation used above, set  $g = \gamma, m = \mu, l = \lambda, u_o = u_o, K_o = K_o$ .)

Figure 1:

Ocean surface current (see equation (20)) assuming  $\mu = 1/200$  1/m,  $\lambda = 2\pi \times 10^{-5}$  1/m, and  $u_o = 1$  m/s.

Figure 2:

Induced horizontal magnetic field  $B_x$  due to velocity profile shown in Figure 1 calculated from equation (32) assuming  $\gamma = 1/5000$  1/m,  $\sigma_o = 5$  S,  $F_z = -3 \times 10^{-5}$  T, and  $F_y = 3 \times 10^{-5} T$ .

Figure 3:

Induced horizontal magnetic field  $B_x$  due to velocity profile shown in figure 1 calculated from equation (32) assuming  $\gamma = 1/5000$  1/m,  $\sigma_o = 5$  S,  $F_z = 0$ , and  $F_y = 3 \times 10^{-5} T$ .

Figure 4:

Electromagnetic fields calculated as described in §3.2 assuming  $\gamma = 0$ ,  $\mu = 1/500$  1/m. In (a) the prescribed velocity and conductivity are shown as solid and dashed lines respectively.

Figure 5:

Electromagnetic fields calculated as described in §3.2 assuming  $\gamma = 0$ ,  $\mu = 0$  (barotropic current).

Figure 6:

Electromagnetic fields calculated as described in §3.2 assuming  $\gamma = 0$ ,  $\mu = \frac{i\pi}{H}$  1/m.

Figure 7:

Electromagnetic fields calculated as described in §3.2 assuming  $\gamma = 1/(5 \times 10^3)$  1/m,  $\mu = 1/500$  1/m.

Figure 8:

Electromagnetic fields calculated as described in §3.2 assuming  $\gamma = 1/(5 \times 10^3)$  1/m,  $\mu = \frac{i\pi}{H}$  1/m.

Figure 9:

Electromagnetic fields calculated as described in §3.2 assuming  $\gamma = 1/(5 \times 10^3)$  1/m,  $\mu = \frac{i2\pi}{H}$  1/m.

Figure 10:

An example (described in text) of the vertical coordinate  $s$  (b), and induced magnetic field  $b_x$  (c), calculated assuming the velocity and conductivity profiles shown in (a). The sediment layer extends down to  $h = -3H$ . (In (a) the vertical scale is only shown to  $z = -1.5 H$ .)

Figure 11:

The stream function  $\psi$  (a), and northward velocity  $v$  (b) for a Stommel gyre (described in text §4.2.1).

Figure 12:

The vertical magnetic component  $b_z$  (calculated from equation (66) at an altitude  $z = 10$  km) induced by the Stommel gyre shown in figure 11.

Figure 13:

Real part of ocean current velocity field (67) with  $l = 0$  and  $k = 2\pi/2000$  1/km. (See §4.2.1 for further details.)

Figure 14:

Induced vertical magnetic field  $b_z$  at  $z = 0$  calculated from (69) due to ocean currents shown in Figure 13. (See §4.2.1 for further details.)

Figure 15:

Ocean current velocity vectors for a field of gyres. (See §4.2.1 for further details.)

Figure 16:

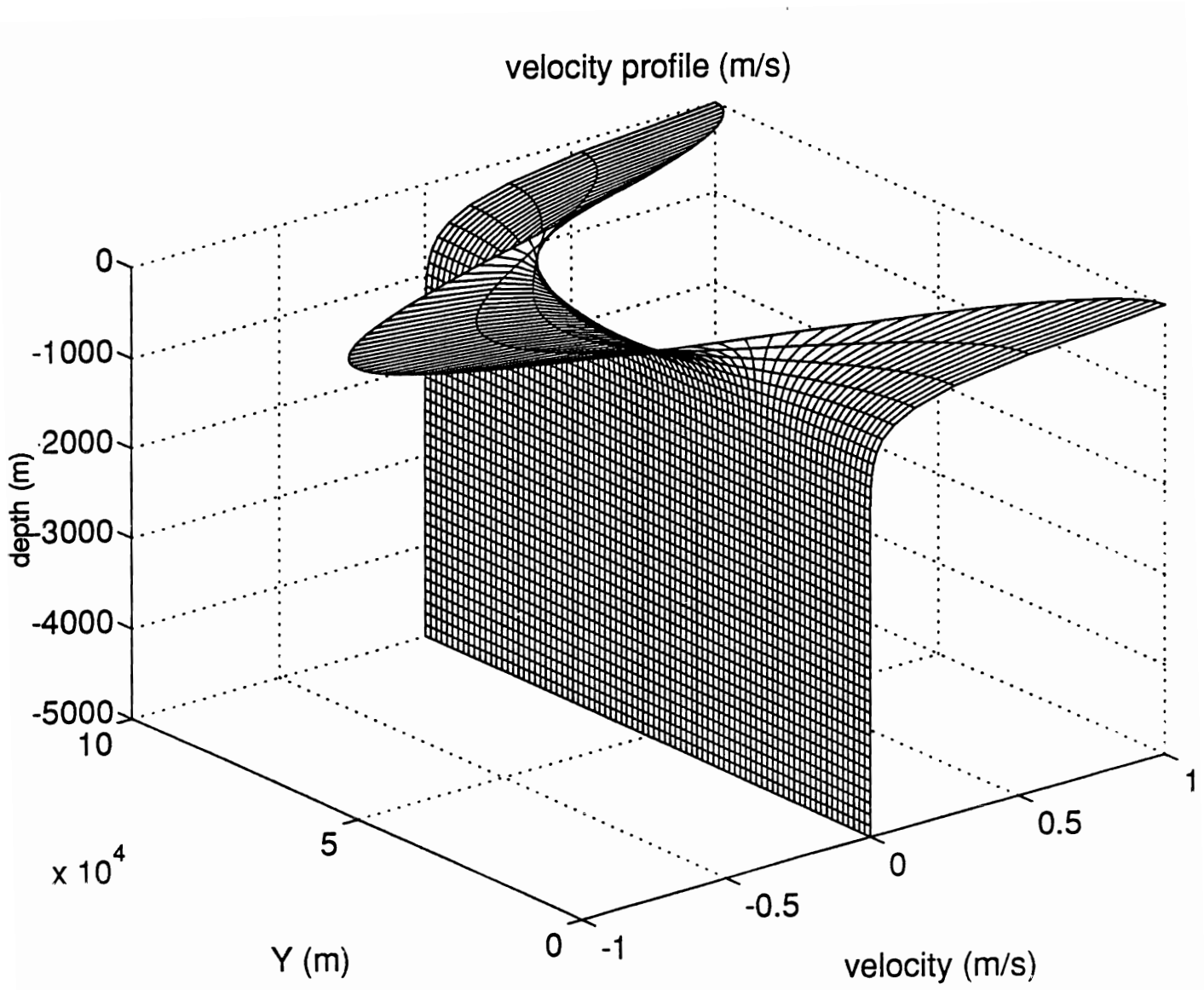
Induced vertical magnetic field  $b_z$  at  $z = 0$  due to ocean currents shown in Figure 15. (See §4.2.1.)

Figure 17:

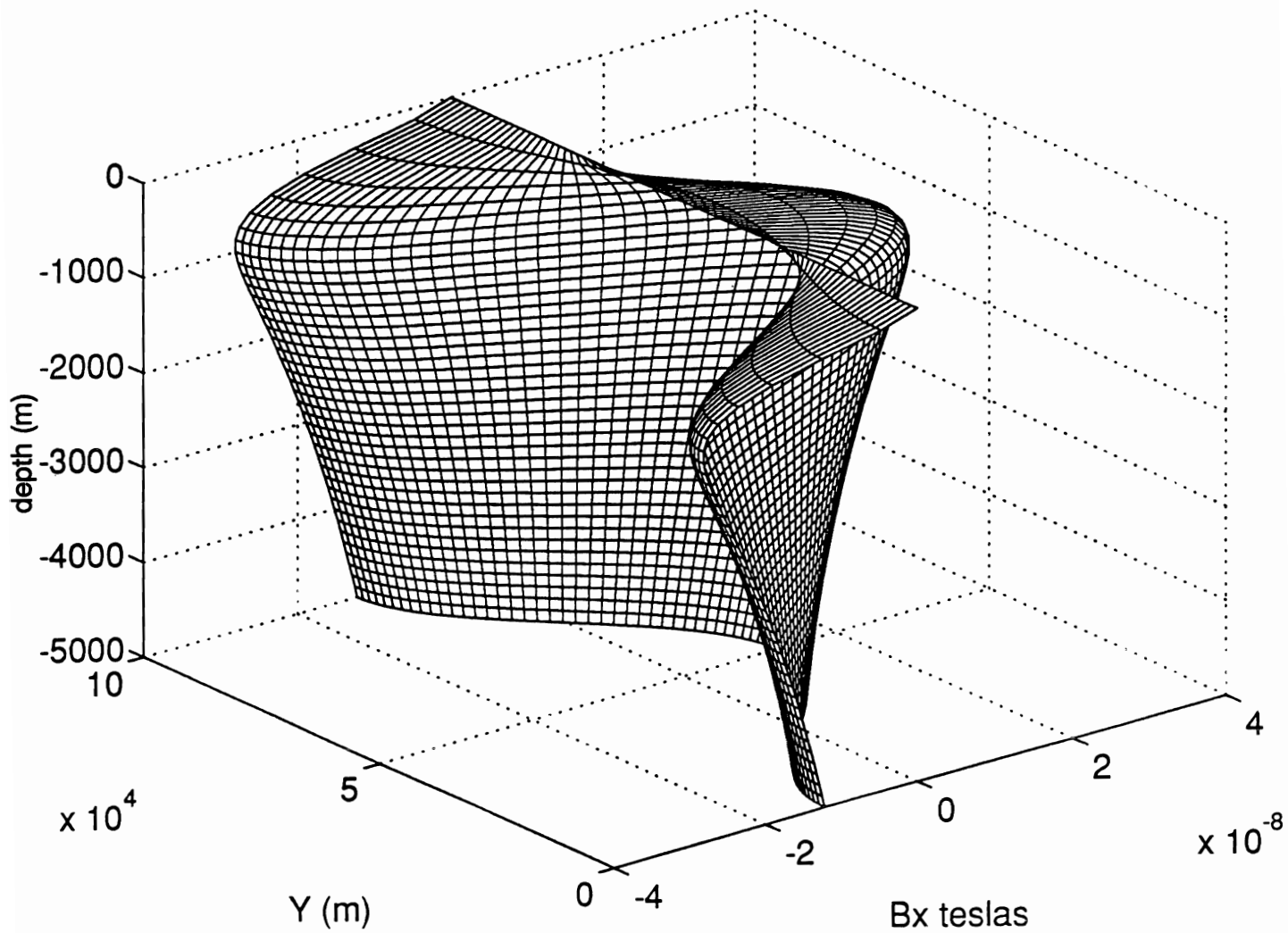
The amplitude of the induced vertical magnetic field  $b_z$  at  $z = 0$  (i.e.,  $\frac{v_o \beta_m}{2K \kappa^2} (1 - e^{-\kappa D})$ ) as a function of the wavelength ( $= 2\pi/\kappa$ ) and thickness  $D$  of the ocean current features seen in either figures 14 or 16.

Figure 18:

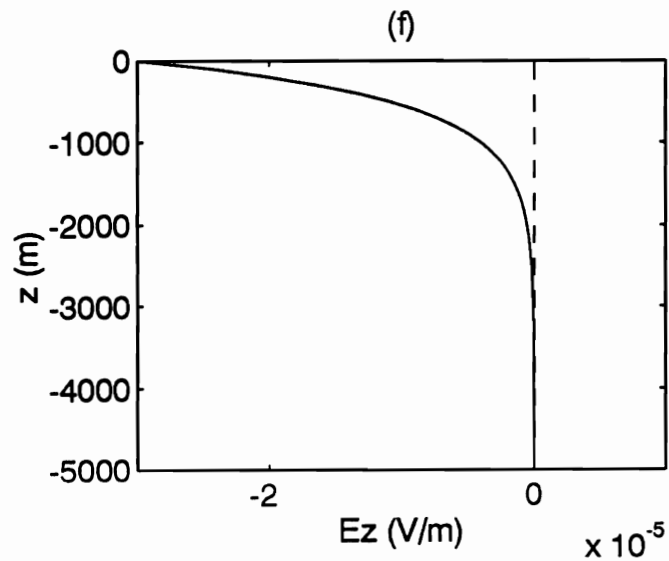
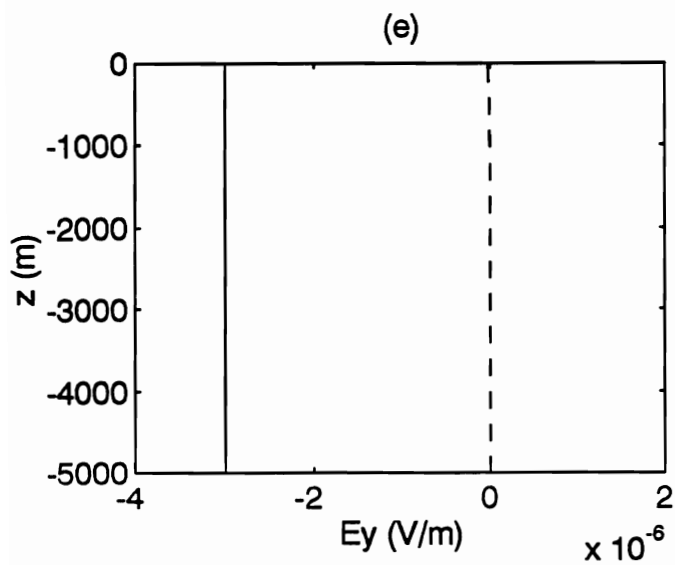
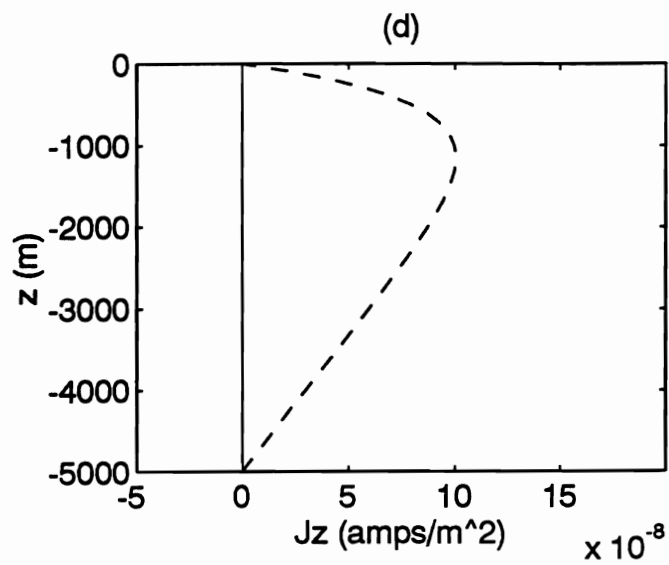
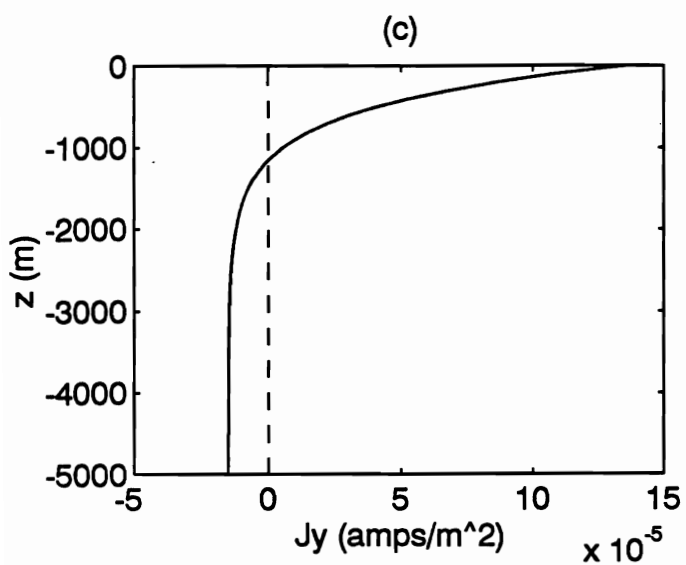
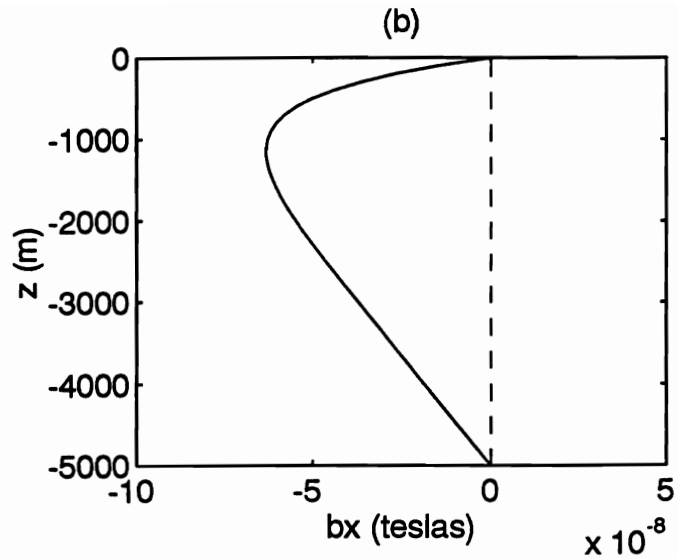
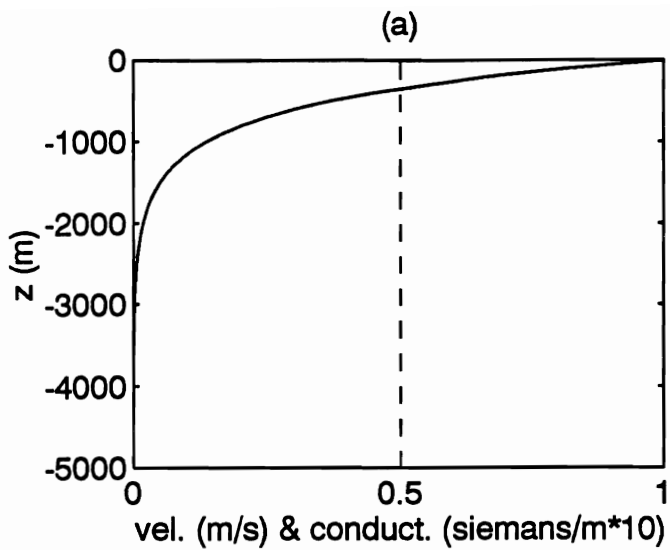
The vertical component of the earth's magnetic field  $F_z$  as determined from spherical harmonic coefficients based on MAGSAT observations (courtesy of Robert Langel). Here we use the convention that positive values correspond to an upward directed field. Units are nT.

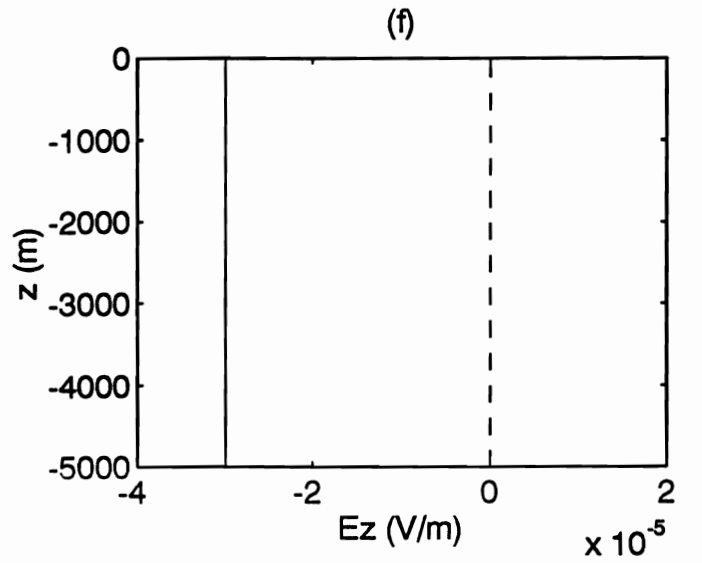
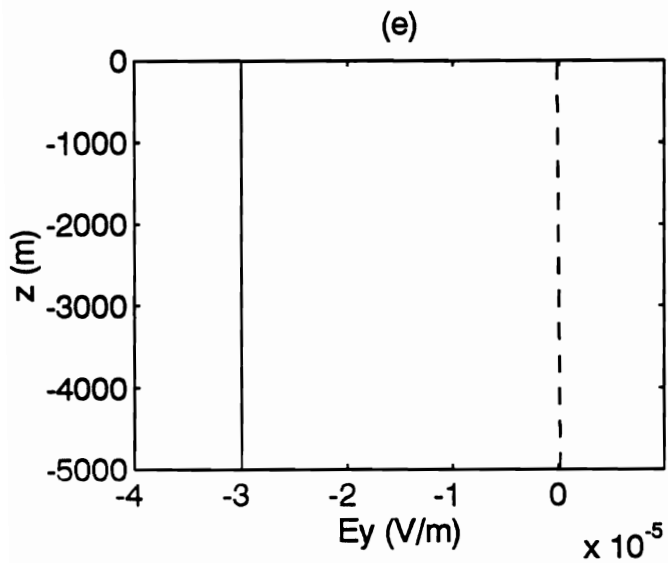
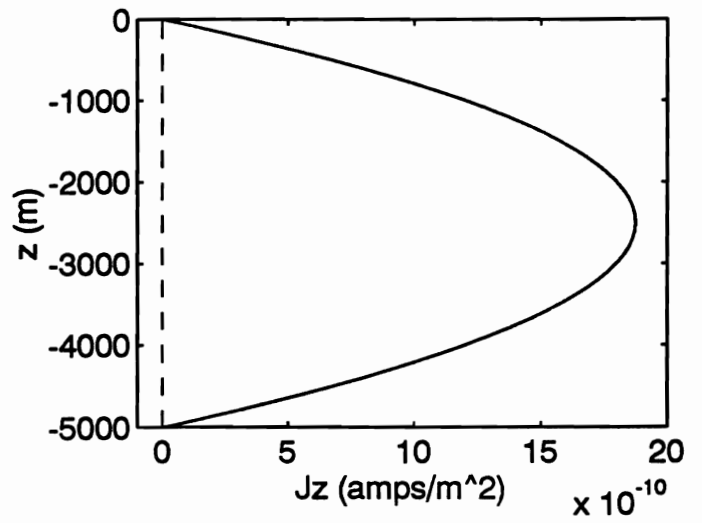
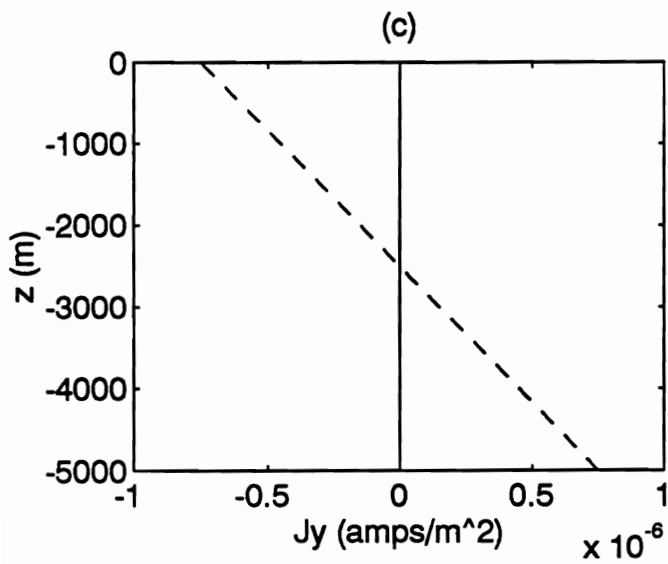
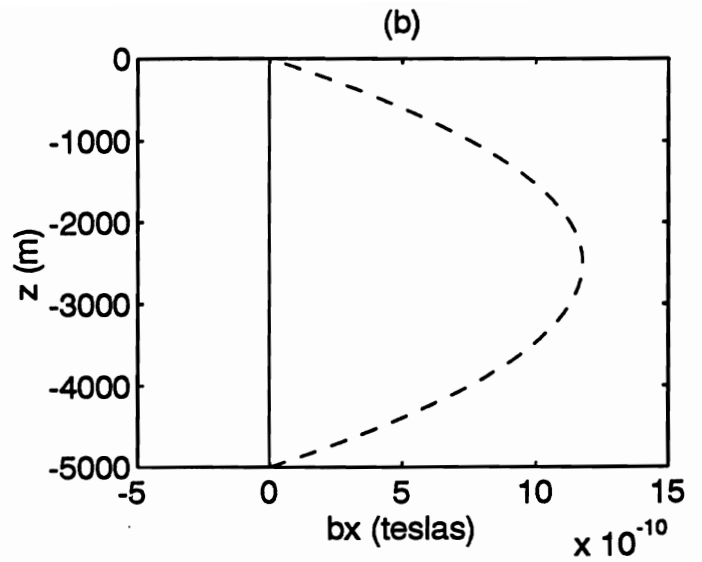
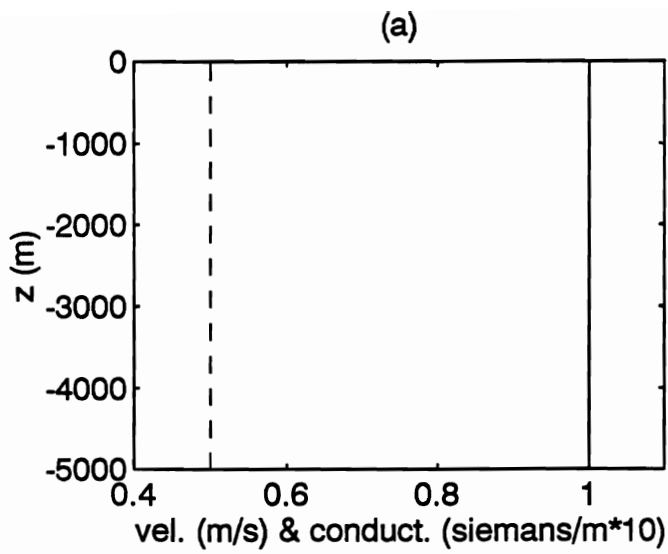


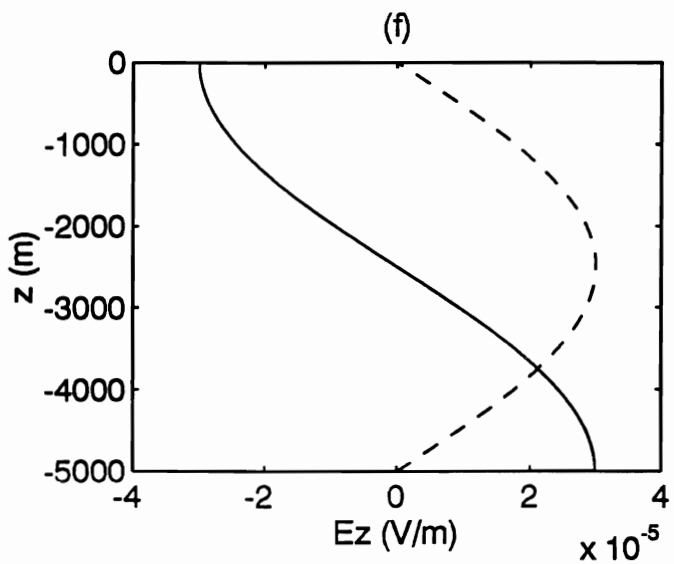
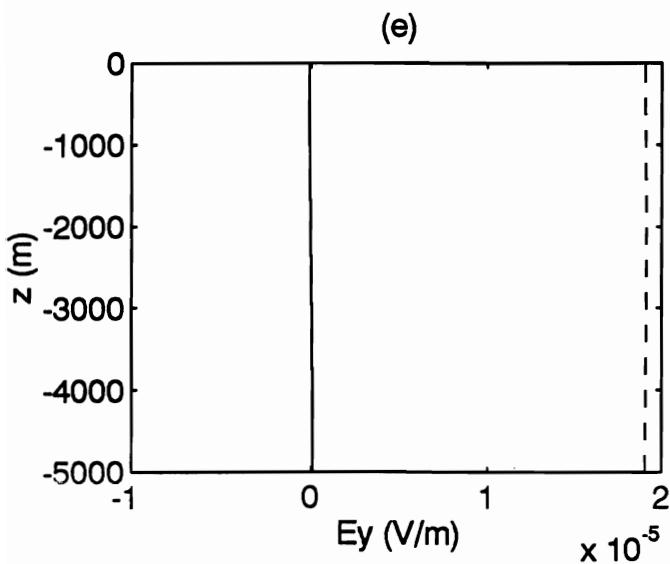
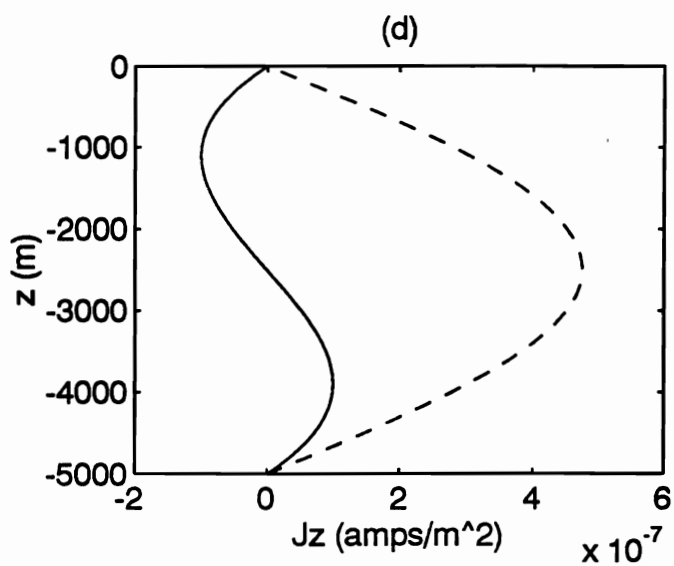
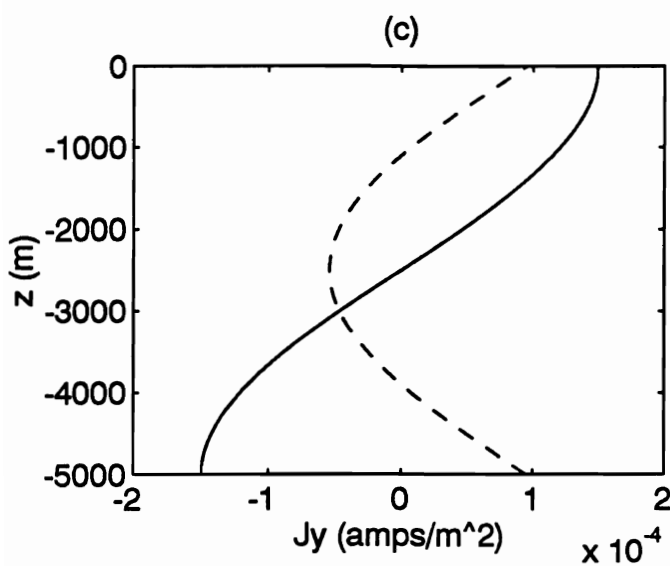
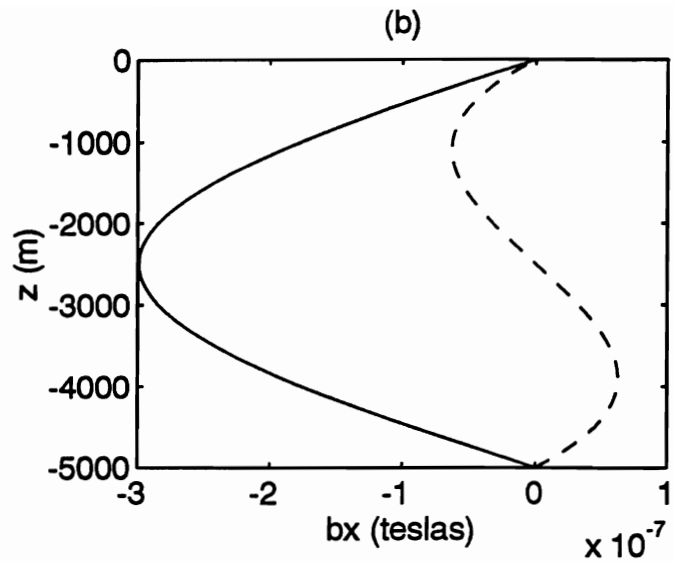
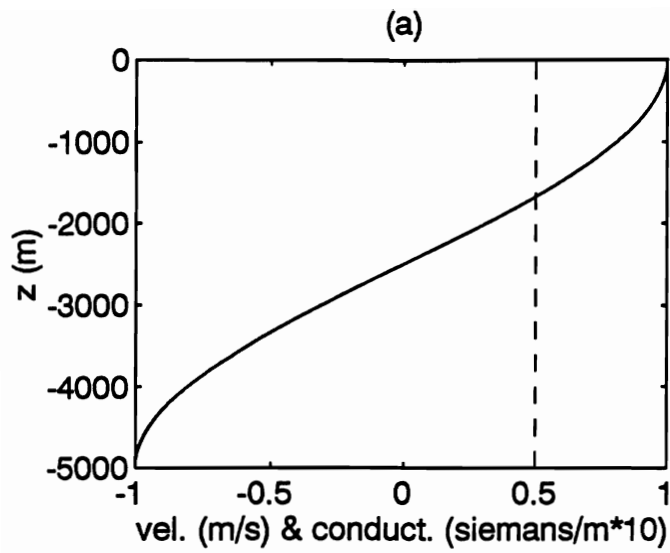
gamma=1/5000

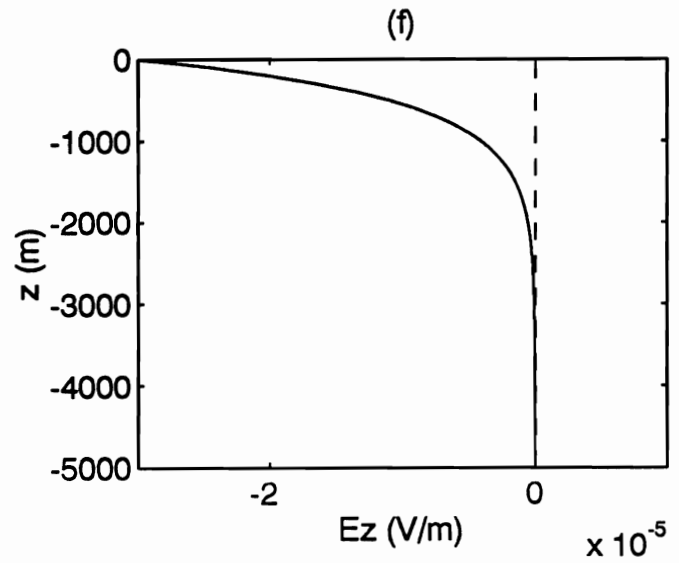
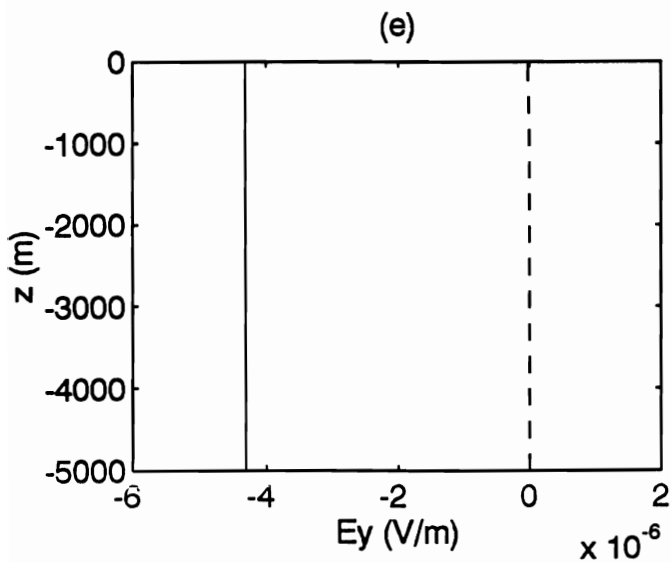
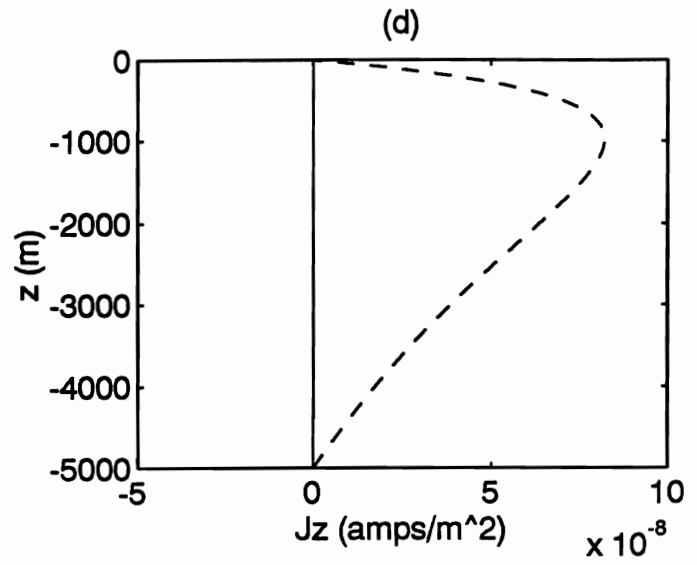
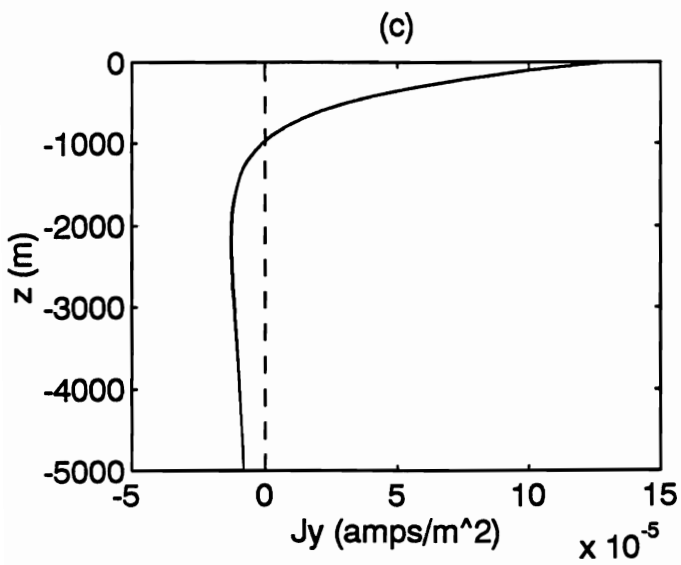
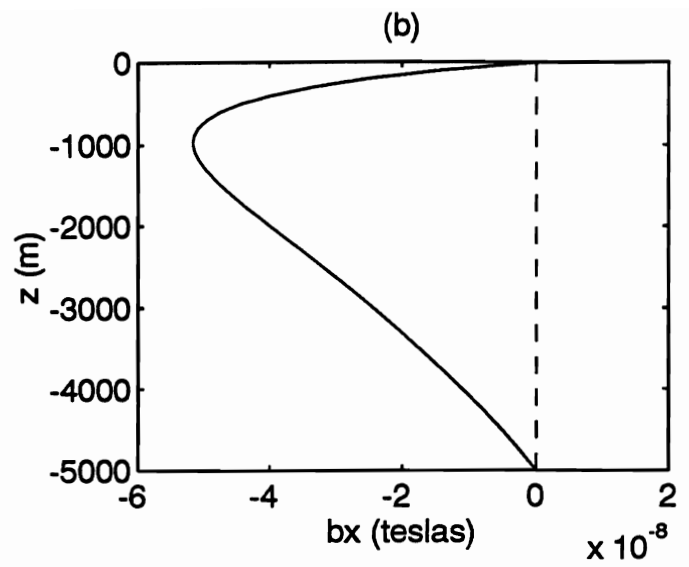
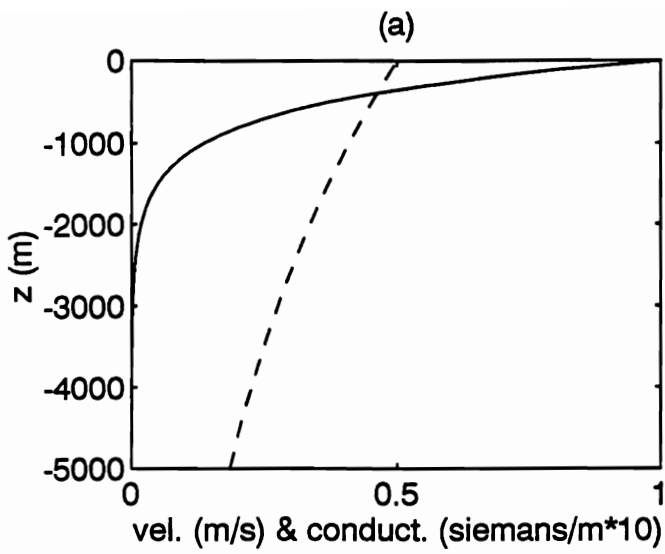


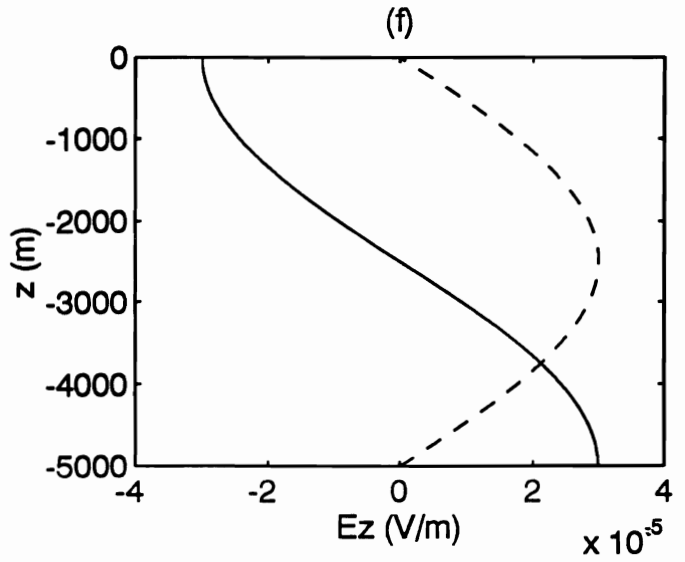
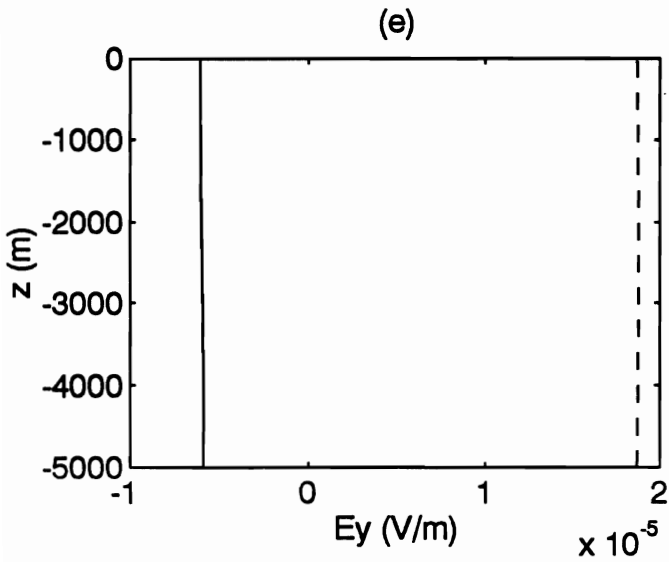
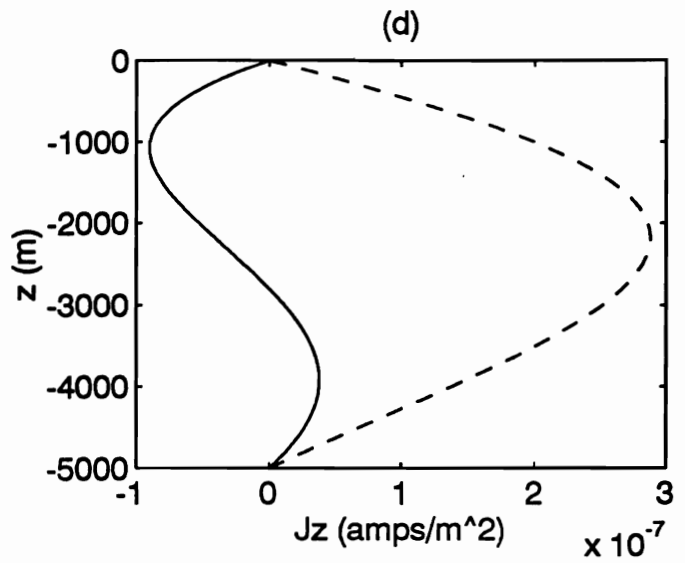
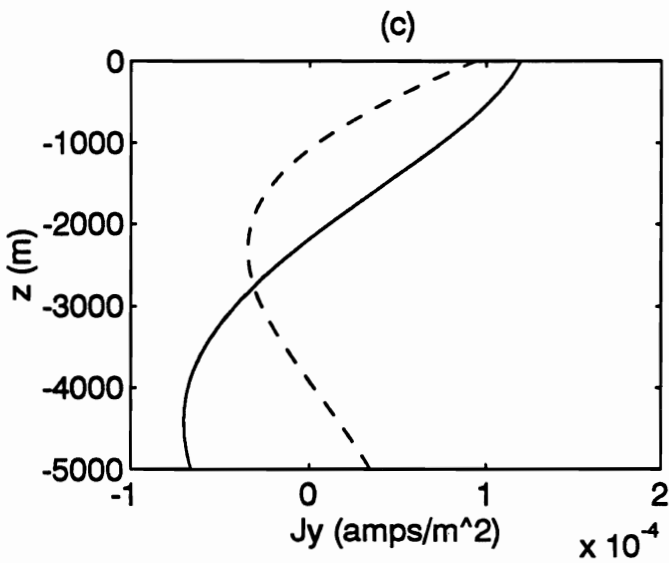
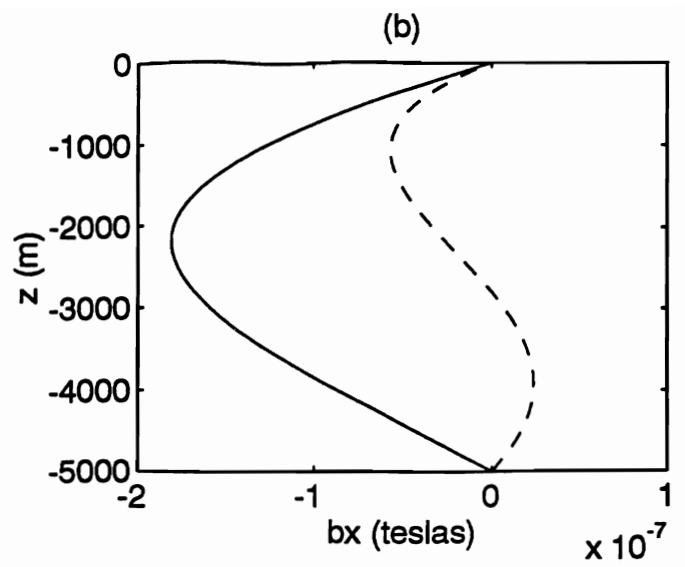
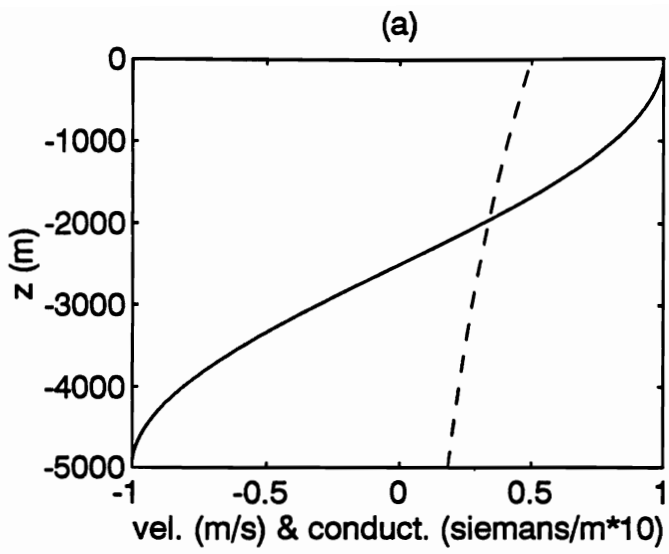


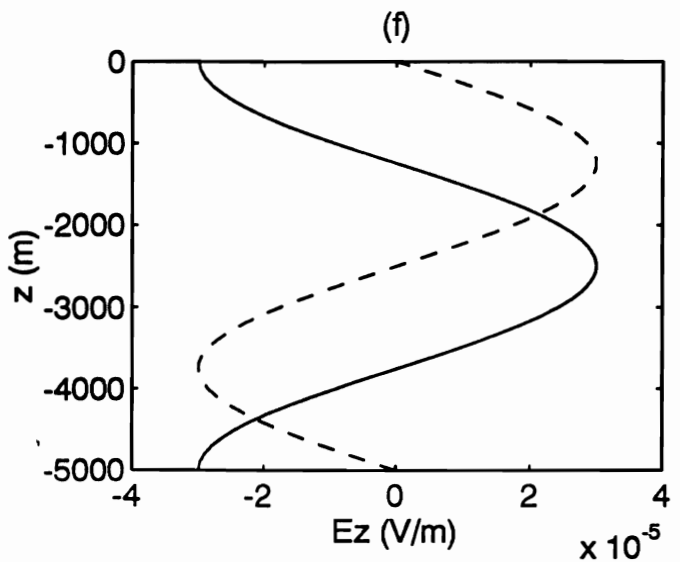
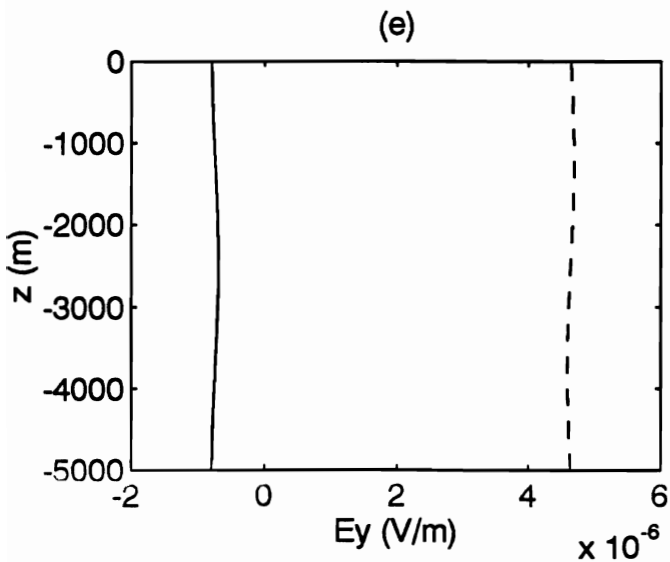
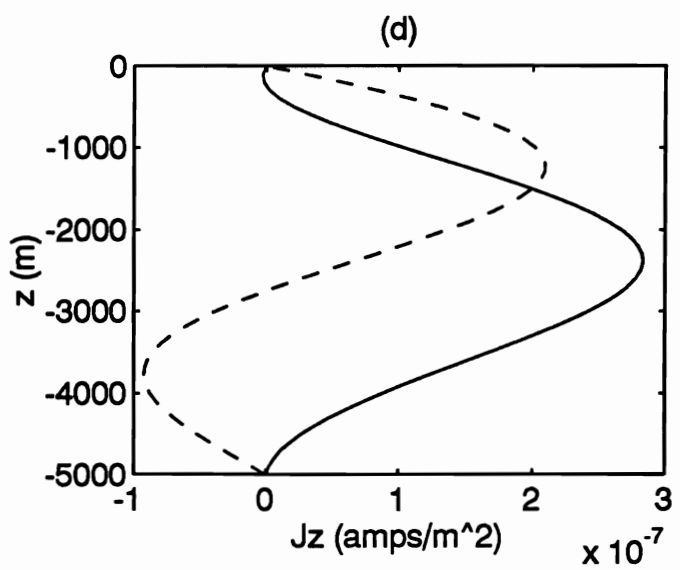
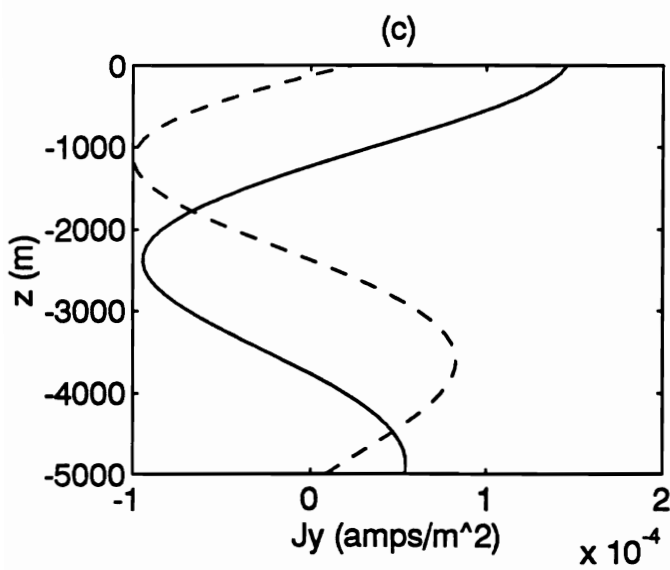
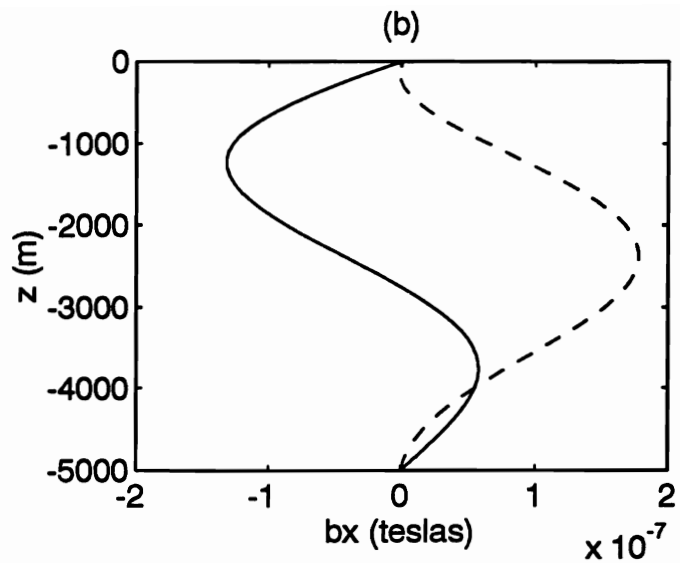
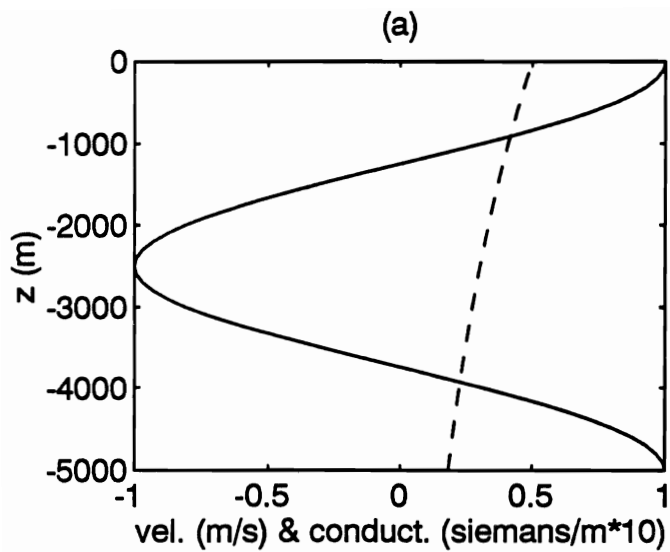


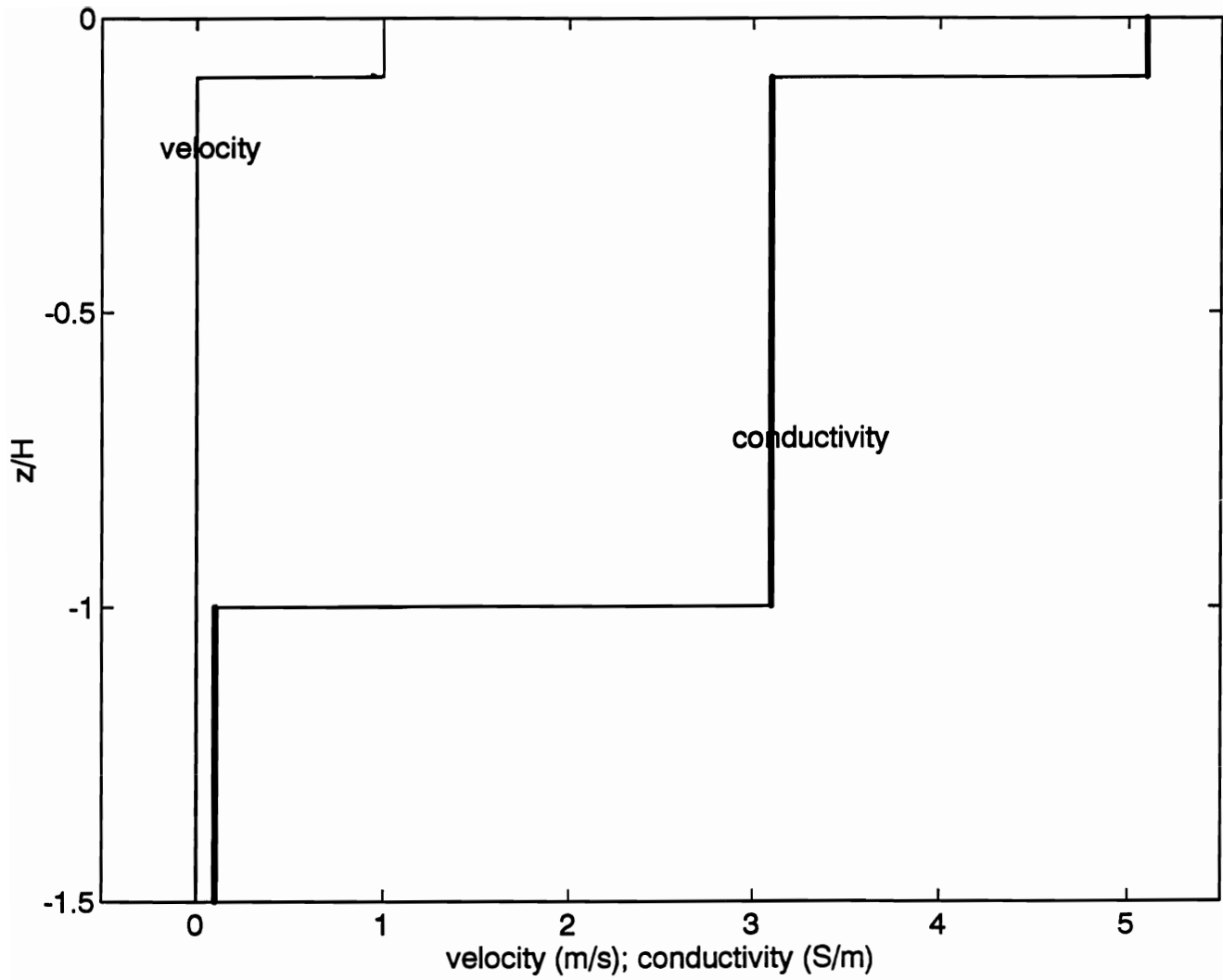


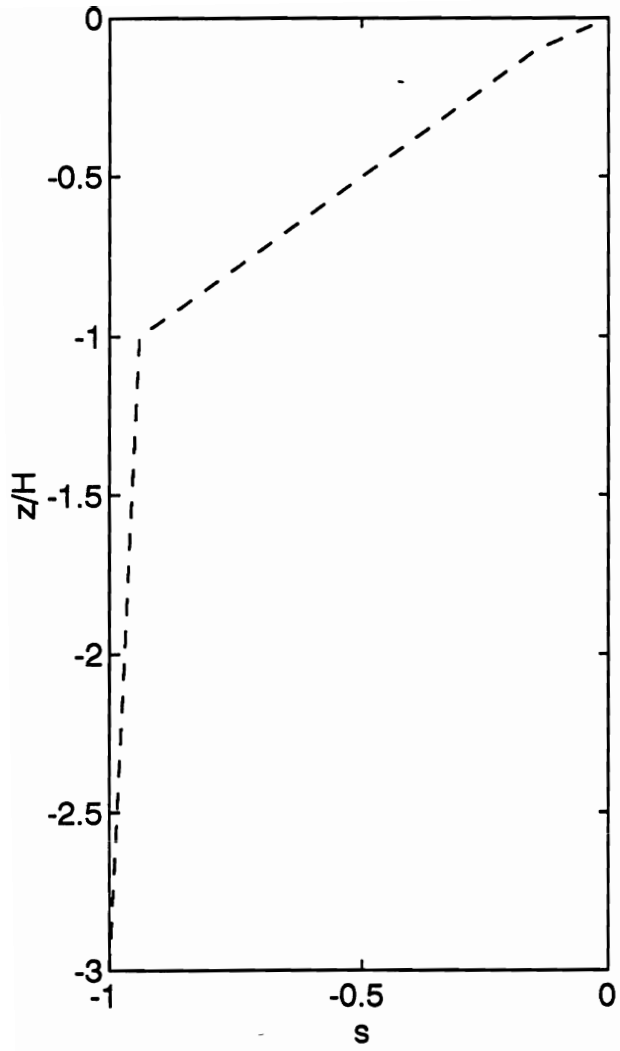




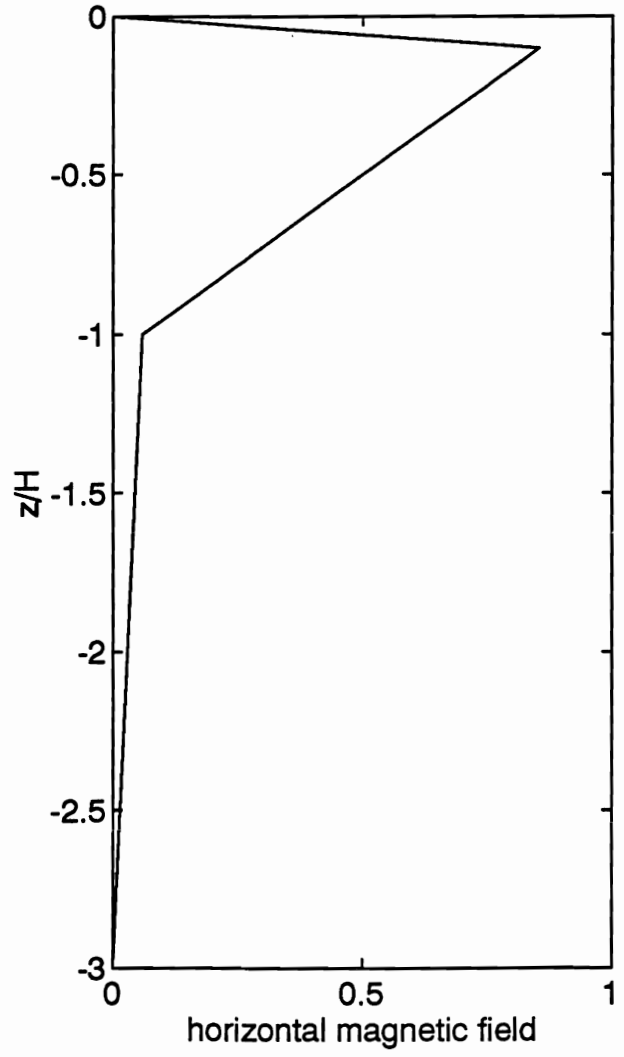








b



c

